Crystallization and Disturbance Histories of Single Zircon Crystals From Hadean-Eoarchean Acasta Gneisses Examined by LA-ICP-MS U-Pb Traverses

Martin Guitreau, Nicolas Mora, Jean-Louis Paquette

AGU PUBLICATIONS

Geochemistry, Geophysics, Geosystems

RESEARCH ARTICLE
10.1002/2017GC007310

Key Points:
- Traverses done by laser-ablation-inductively coupled-plasma mass spectrometry can help isolate zones with coherent isotope systematics
- Isolated zones from the same zircon allow crystallization age to be retrieved using internal Discordia lines even for discordant data
- The applicability of traverses is evidenced by zircons from Acasta gneisses that were analyzed in this study

Supporting Information:
- Supporting Information S1
- Figure S1
- Figure S2
- Table S1
- Table S2
- Table S3
- Table S4

Correspondence to:
M. Guitreau,
martin.guitreau@uca.fr

Citation:
Guitreau, M., Mora, N., & Paquette, J.-L. (2018). Crystallization and disturbance histories of single zircon crystals from Hadean-Eoarchean Acasta gneisses examined by LA-ICP-MS U-Pb traverses. *Geochemistry, Geophysics, Geosystems*, *19*, 272–291. https://doi.org/10.1002/2017GC007310

Received 2 NOV 2017
Accepted 20 DEC 2017
Accepted article online 8 JAN 2018
Published online 25 JAN 2018

Crystallization and Disturbance Histories of Single Zircon Crystals From Hadean-Eoarchean Acasta Gneisses Examined by LA-ICP-MS U-Pb Traverses

Martin Guitreau[1], Nicolas Mora[1], and Jean-Louis Paquette[1]

[1]Université Clermont Auvergne, CNRS, IRD, OPGC, Laboratoire Magmas et Volcans, Clermont-Ferrand, France

Abstract Zircon U-Pb geochronology is a very robust dating method but the accuracy of determined ages can sometimes be compromised. This is because, as commonly observed, the U-Pb isotope system can be reopened during the post-crystallization evolution of a zircon. The present manuscript investigates the capability of traverses by LA-ICP-MS to identify zones of well-preserved U-Pb isotope systematics within zircon crystals. The data for the different zones can be used to construct internal Discordia lines that provide age information about crystallization and metamorphism of single zircon crystals. To test our approach, we analyzed zircons from three ca. 3.96 Ga Acasta gneisses. Results demonstrate that such a method allows retrieval of original crystallization age in most of the studied zircons, even in those that experienced ancient U-Pb disturbances resulting in discordant U-Pb data. It was also possible to estimate disturbance ages, though not as precisely as for the igneous crystallization, in many of the studied crystals.

1. Introduction

Zircon U-Pb geochronology is probably the most reliable dating technique in Earth Sciences. It has two major advantages. First of all, the U-Pb isotope system includes two chronometers with distinct half-lives and that have parents and daughters made of the same chemical elements (e.g., Schoene, 2014). This means that disturbances affecting the U-Pb systems can only result in decoupling of daughters from parents (e.g., ^{206}Pb from ^{238}U) but not parents nor daughters from each other (i.e., ^{238}U from ^{235}U or ^{206}Pb from ^{207}Pb). As a consequence, the two chronometers remain chemically coupled but can be temporally decoupled, as often seen (e.g., Corfu, 2013; Wetherill, 1963). However, even when there is evidence for decoupling, meaningful age information can sometime be retrieved by using Discordia lines in Concordia diagrams, which can indicate the age of original crystallization and that of U-Pb system reopening, or allow deconvolution of mixtures between age components (e.g., Allègre, 1967; Amelin et al., 1999, 2000; Catanzaro & Kulp, 1964; Guitreau & Blichert-Toft, 2014; Schoene, 2014; Wetherill, 1956). The second advantage of zircon U-Pb geochronology arises out of zircon's refractory and retentive nature such that it survives most geological processes (e.g., crust reworking, weathering, erosion) and most chemical elements diffuse very slowly in zircon's crystal lattice (e.g., Cherniak & Watson, 2003). Good examples of this preservation capability are provided by up to 4.38 Ga Jack Hills detrital zircons (e.g., Harrison, 2009), 4.0 Ga Acasta gneiss zircons (e.g., Stern & Bleeker, 1998), and 3.9 Ga Napier complex zircons (e.g., Black et al., 1986), the latter of which experienced two ultrahigh-temperature granulite events.

However, zircon has also long been known to imperfectly preserve its lattice over time (e.g., Holland & Gottfried, 1955; Murakami et al., 1991), which is a direct consequence of what makes zircon interesting for geochronology, namely its high U and Th contents. Radioactive U and Th isotopes inevitably decay over time inducing defect formation and bond destruction through emissions of high energy alpha-particles and nuclei recoil chains (e.g., Ewing et al., 2003). Therefore, despite zircon being a very robust information-keeper, it can be sensitive to thermal events resulting in a (partial) loss of chemical and/or isotopic information. However, zircon can also record thermal events through recrystallization and/or formation of overgrowths (e.g., Möller et al., 2003). This behavior is directly responsible for some of the complexities observed in ancient zircon crystals (e.g., Kusiak et al., 2013a, 2013b; Pidgeon et al., 2017; Valley et al., 2015). Plastic and seismically induced deformation can also affect the U-Pb isotope systems as pointed out by Timms et al. (2006) and Kovaleva and Klötzli (2017).

Despite the excellent spatial resolution that microbeam techniques can achieve in the present-day, dating methods commonly do not allow the full potential of U-Pb information in zircon to be exploited. This is because either part of the variability in U-Pb ages is an artifact of the dating approach or because only the most concordant data are taken into account as they are easier to interpret. However, U-Pb systems can retain the memory of multiple events which can only be retrieved when meaningful Discordia lines are established (e.g., Schoene, 2014). This implies that one U-Pb analysis cannot unambiguously depict the crystallization age of a zircon, unless it is fully concordant. Yet, even very limitedly discordant data can result in the establishment of inaccurate crystallization ages (e.g., Corfu, 2013; Guitreau & Blichert-Toft, 2014; Williams et al., 1984). In the search for Concordance, a large number of U-Pb data are commonly discarded. This is a critical issue for ancient crystals because they are even more prone to lattice damaging and disturbances than younger ones, such that only a small subset of all analyzed zircons exhibit concordant data. This issue is even more critical for detrital zircons (e.g., Amelin et al., 2000; Gehrels, 2014; Guitreau & Blichert-Toft, 2014) as some populations can be completely avoided and hence go unidentified because they are too discordant. Zircon texture as revealed by CL and BSE images is an excellent indicator of crystal magmatic and metamorphic history (e.g., Corfu et al., 2003), and, to a first-order, a good proxy of U-Pb concordance (e.g., Connelly, 2001) but many examples, especially in ancient zircons, show that crystal texture does not unambiguously discriminate between disturbed and undisturbed domains (e.g., Valley et al., 2015). Another problem deals with the analytical volume inherent in spot-mode LA-ICP-MS analysis because while the laser spot may be centrally placed within a zone observed in CL, there is no guarantee that it remains within that zone as it bores into the crystal. Examination of the data on a cycle-by-cycle basis can minimize, but not eliminate this problem fully given that there could be domains of similar age but with different U-Pb systematics. (e.g., Zirakparvar, 2015; Zirakparvar et al., 2017). Dating zircon multiple times, and in different locations, can enable internal Discordia lines to be identified (e.g., Guitreau & Blichert-Toft, 2014), and if the zircon history is not too complex, these lines, contrary to single spots, can reveal actual crystallization and disturbance ages.

In this contribution, we have tested the capability of U-Pb traverses by LA-ICP-MS to decipher ancient zircon crystallization and disturbance histories at the scale of single crystals. A major advantage of traverses, compared to spot analyses, is that zircon textures, as revealed by CL and BSE images, can be more accurately associated to the collected U-Pb data because of the shallower excavation of the laser during traverses compared to spot analyses. In addition, data acquisition with LA-ICP-MS traverses is not dictated by a user's interpretation of which part of a crystal is the most likely to reveal valuable age information. In contrast, zircon, itself, exposes this information that can subsequently be put in relation with the observed texture, and not the other way around. In practice, age patterns can be followed throughout crystals, hence, revealing if zones with distinct U-Pb systematics are present. If multiple zones exist within a crystal, their corresponding U-Pb data can be isolated from the traverse's signal and considered as independent data sets because of the negligible downhole fractionation that occurs during LA-ICP-MS rastering (e.g., Košler & Sylvester, 2003). When plotted together on a Concordia plot, data for different zones within a same crystal can provide information regarding the crystallization and the disturbance histories of the analyzed crystal. This traverse-based approach provides a time effective alternative to the more labor intensive method of taking the zircon crystal out of the mount once it has been analyzed, and then sectioning it to examine the analytical volume in relation to the CL/BSE image (e.g., Zirakparvar, 2015; Zirakparvar et al., 2017). To test our U-Pb dating approach, we analyzed zircons from Acasta gneisses because they are well-documented examples of ancient zircon populations that exhibit complex U-Pb patterns (e.g., Bauer et al., 2017; Bowring & Williams, 1999; Guitreau et al., 2012, 2014; Iizuka et al., 2007, 2009; Mojzsis et al., 2014; Reimink et al., 2014, 2016; Stern & Bleeker, 1998). These complexities are, nevertheless, well-documented and commonly interpreted as artifacts of multistage ancient and recent Pb-loss, as well as recrystallization and formation of zircon overgrowths during distinct metamorphic events (e.g., Bowring & Williams, 1999; Guitreau et al., 2012; Mojzsis et al., 2014; Sano et al., 1999). In addition, the magmatic and metamorphic history of the Acasta Gneiss Complex (AGC) is understood well-enough (e.g., Iizuka et al., 2007; Reimink et al., 2016) so that ages determined using our approach can be compared to known events in the AGC, and in turn validate the use of U-Pb traverses by LA-ICP-MS to unravel crystallization and metamorphic histories of single zircon crystals.

2. The Magmatic and Metamorphic Record of the Acasta Gneiss Complex

The Acasta Gneiss Complex (AGC) is a small (~20 km^2) crustal domain that is located in the Northwest Territories of Canada and it crops out on the western edge of the Slave craton (Figure 1). Rocks making up the AGC are essentially orthogneisses with dioritic to granitic compositions. They are in low strain in the eastern part of the complex and in high strain in the western part (Bowring et al., 1989; Bowring & Williams, 1999; Iizuka et al., 2007). Minor amphibolites can also be found as centimeter to kilometer-scale enclaves throughout the AGC (e.g., Iizuka et al., 2007; Koshida et al., 2016; Reimink et al., 2016).

The AGC was accidentally discovered during a reconnaissance campaign for the Wopmay Orogen in the 1980s (King, 1986). The AGC was initially studied by Sam Bowring who proposed a crystallization age of 3,962 ± 3 Ma for the protolith to the oldest gneisses based on zircon U-Pb ages measured by SHRIMP (Sensitive High Resolution Ion Microprobe; Bowring et al., 1989). During the 1990s, the Geological Survey of Canada (GSC) launched large-scale campaigns for the study of the Slave craton which notably resulted in a deeper understanding of the AGC geological history (Bleeker & Davies, 1999; Bleeker & Stern, 1997). During these studies, Stern and Bleeker (1998) pushed the crystallization age of the oldest protolith to Acasta gneisses back to 4,025 ± 15 Ma (2σ) also using zircon U-Pb geochronology by SHRIMP. Shortly after, Bowring and Williams (1999) also discovered very old zircon ages that they similarly interpreted as the age of the protolith to the studied Acasta gneisses, which gave 4,002 ± 4, 4,012 ± 6, and 4,031 ± 3 Ma (1σ). The above-mentioned studies, together with Hodges et al. (1995) and Sano et al. (1999), have documented several magmatic and metamorphic events using U-Pb geochronology applied to zircon and apatite, as well as $^{40}Ar/^{39}Ar$ ages on hornblende and biotite (Table 1).

In spite of detailed geochronology, the origin of the AGC remained enigmatic, notably concerning the sources involved in its formation. The Sm-Nd isotope analyses performed in the 1990s to tackle this issue were

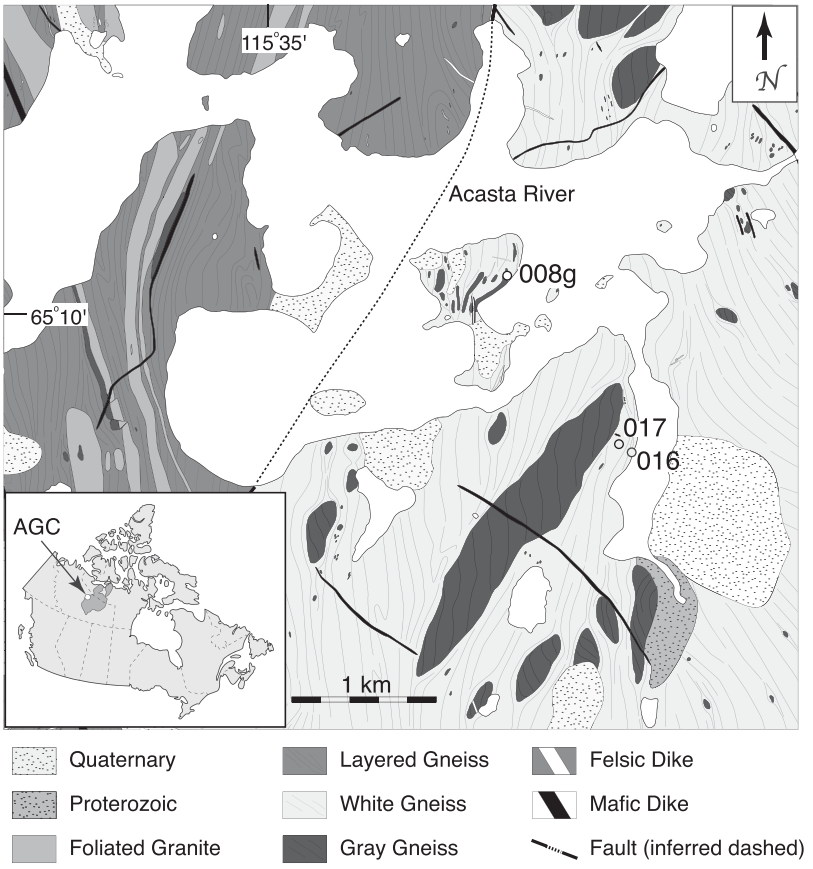

Figure 1. Geological map of the Acasta Gneiss Complex (AGC) with detail of sampling locations (after Iizuka et al., 2007; Mojzsis et al., 2014). The inset shows the location of the AGC relative to Canada.

Table 1
Summary of Geological Events That Occurred at the Acasta Gneiss Complex

Episode #	Age (Ga)	Geological event	References
1	4,200	Crystallization of the zircon core identified by Iizuka et al. (2006)	*l*
2	4,020–4,000	Formation of the oldest diorites and tonalites	*d, f, h, i, r, s*
3	3,960–3,920	Tonalite formation	*a, b, m, o, p, q, s, t*
4	~3,800	Inherited zircon age	*a, d, g, i, k, m, o, q*
5	~3,750	Granitoid formation	*b, g, k, m, o, q, s, t*
6	3,600–3,550	Anatexis and granitoid formation	*b, d, g, i, k, m, o, p, q, s, t*
7	3,400–3,350	Regional metamorphism and granitoid formation	*d, e, i, m, q, s, t*
8	3,150–3,100	Regional metamorphism	*d*
9	2,950–2,900	Regional metamorphism, granitoid formation, garnet formation	*d, s, t*
10	2,550–2,600	Granite intrusion	*h*
11	1,900–1,800	Wopmay orogen	*c, i, j*

Notes. References are as follows: (a) Bowring et al. (1989); (b) Bowring and Housh (1995); (c) Hodges et al. (1995); (d) Bleeker and Stern (1997); (e) Moorbath et al. (1997); (f) Stern and Bleeker (1998); (g) Amelin et al. (1999); (h) Bleeker and Davies (1999); (i) Bowring and Williams (1999); (j) Sano et al. (1999); (k) Amelin et al. (2000); (l) Iizuka et al. (2006); (m) Iizuka et al. (2007); (n) Iizuka et al. (2009); (o) Guitreau et al. (2012); (p) Guitreau et al. (2014); (q) Mojzsis et al. (2014); (r) Reimink et al. (2014); (s) Reimink et al. (2016); (t) Bauer et al. (2017).

somewhat inconclusive because debates existed regarding the pristineness of the Sm-Nd isotope systematics in the Acasta gneisses (Bowring & Housh, 1995; Moorbath et al., 1997). Amelin et al. (1999, 2000), presented the first Lu-Hf isotope data for Acasta gneiss zircons and identified significant involvement of an enriched reservoir in the AGC formation at ~3.8, ~3.7, and ~3.6 Ga. However, they did not analyze zircons belonging to the oldest recognized events (>3.9 Ga). In the late 2000s, a Japanese group revisited the AGC. They produced a detailed map, refined the known magmatic and metamorphic history of the AGC (Iizuka et al., 2007), and presented Lu-Hf isotope analyses by LA-MC-ICP-MS for numerous zircons that led them to conclude that even the oldest Acasta gneisses contained a reworked Hadean crustal component (Iizuka et al., 2009). The Japanese group also identified an inherited zircon core dated at 4.2 Ga (Iizuka et al., 2006), which is the only Hadean zircon so far discovered in a meta-igneous sample. Following the work of Iizuka et al. (2006, 2007, 2009), a group led by Steve Mojzsis published a series of paper in which it was shown that both juvenile and reworked sources were involved, and that some Acasta gneisses preserved negative ^{142}Nd and positive ^{182}W anomalies (Guitreau et al., 2014; Mojzsis et al., 2014; Roth et al., 2014; Willbold et al., 2015). Most recently, a group led by Tom Chacko tackled the issue of the context of formation of the AGC and proposed that it started out as a mafic plateau, analogous to Iceland, 4.02 Gyr ago and evolved by shallow crustal processes until 3.6 Ga when voluminous TTGs were generated, perhaps in a subduction-like setting (Reimink et al., 2014, 2016). This group obtained a concordant ID-TIMS zircon age of 4,013.7 ± 0.3 Ma (Reimink et al., 2016), that they propose represent the best age estimate for the oldest component of AGC magmatism. Finally, Bauer et al. (2017) presented laser-ablation split-stream Lu-Hf and U-Pb isotope data for Acasta gneiss zircons that reveal a major change in the source of AGC rocks at about 3.6 Ga, with the involvement of juvenile material, and the progressive disappearance of the >4.0 Ga crustal signature. A summary of the magmatic and metamorphic history of the AGC derived from the studies presented above is given in Table 1.

3. Analytical Details

3.1. U-Th-Pb Dating of Zircon by LA-ICP-MS Traverses

Prior to analysis, zircons from three Acasta samples (AG09008g, AG09016, and AG09017) previously analyzed by Guitreau et al. (2012) were handpicked, mounted in epoxy, and imaged by cathodoluminescence (CL) as well as by back-scattered electrons (BSE) using a Jeol JSM-5910LV scanning electron microscope at the Laboratoire Magmas et Volcans (LMV, Université Clermont Auvergne, Clermont-Ferrand, France). During both CL and BSE image acquisition, the acceleration voltage was set to 15 kV. Zircon internal textures, as revealed by CL and BSE images, were used to select crystals to be analyzed by LA-ICP-MS, determine the locations for the traverses, and interpret the resulting data. We mounted and imaged a total of 94, 151, and 53 zircon crystals from AG09008g, AG09016, and AG09017, respectively, and further selected 21, 92, and 19

Table 2
LA-ICP-MS Operating Conditions

Analysis	U-Pb geochronology
ICP-MS model	Agilent 7500
Forward Power	1,350 W
Auxiliary gas (Ar)	~0.8 L/min
Ar sample	~0.8 L/min
Oxide ThO/Th	~0.5%
Additional gas flow (N_2)	3 mL/min
Laser model	Resonetics resolution M-50
Wavelength	193 nm
Pulse duration	< 4 ns
Energy	3.95 mJ
Fluence	2.6 J/cm^2
Frequency	4 Hz
Spot diameter	20 μm
Carrier gas	He
Carrier gas flow	~0.7 L/min
Traverse length	80–100 μm
Traverse rate	~1.5 μm/s or ~0.2 μm/cycle
Traverse depth	3–5 μm
Data acquisition	
Protocol	Time-resolved analysis
Masses measured	202, 204, 206, 207, 208, 232, 238
Settling time	20 μs
Dwell-time per isotope	10–30 ms
Background counting time	20 s
Sample measurement time	60 s
Measurement type	Standard bracketing
External standard	AS3, Plešovice, 91500

zircons, respectively, for LA-ICP-MS analyses. The number of crystals mounted in epoxy was essentially determined by the quantity and quality of zircons available from each sample, whereas the selection for LA-ICP-MS analysis was based on the preservation of magmatic and metamorphic textures and/or the absence of advanced metamictization and alteration features as described in Corfu et al. (2003). Yet, we endeavored to analyze a representative suite of zircon crystals and, hence, no population was purposefully excluded on the basis of appearance, which, in turn, allows the limit of our dating method to be tested.

U-Th-Pb analyses were done at the LMV using a Resonetics Resolution M-50 laser-ablation system coupled to an Agilent 7500 ICP-MS with a dual pumping system (Paquette et al., 2014). LA-ICP-MS operating conditions are given in Table 2. The presence of common Pb was monitored using the ^{204}Pb signal but this latter was not used to correct data because of its poor precision that results from the presence of ^{204}Hg (isobaric interference on ^{204}Pb) in the He gas. When the ^{204}Pb signal was statistically above the background level, data were simply not considered, which happened for 31 traverses. Because of imprecisions inherent to the detection of common Pb at mass 204, we further monitored the presence of common lead by comparing measured ^{232}Th/^{238}U ratios to time-integrated ones calculated from ^{208}Pb/^{206}Pb (e.g., Ireland & Williams, 2003). This technique relies on the fact that ^{208}Pb is the lead isotope that is the most sensitive to common Pb contamination (e.g., Andersen, 2002) and assumes that Pb isotopes in the analyzed zircon account for the measured Th/U. Oxide formation was assessed using the ^{232}Th^{16}O/^{232}Th ratio during measurements of NIST SRM 612 (Table 2). Acasta zircons were analyzed as groups of six that were bracketed by four analyses of the zircon standard 91500 (1,065.4 ± 0.3 Ma; Wiedenbeck et al., 1995) that was used as an external standard. Further, the zircon standards AS3 (1,099.1 ± 0.5 Ma; Paces & Miller, 1993; Schmitz et al., 2003) and Plešovice (337.13 ± 0.37 Ma; Sláma et al., 2008) were also analyzed as unknowns during each session for quality control. All analyses were done as traverses. The terrestrial mean value of 137.818 (Hiess et al., 2012), for the ^{238}U/^{235}U, was used to calculate ^{207}Pb/^{235}U ratios. Age calculations were done using decay constants provided by Jaffey et al. (1971) and LeRoux and Glendenin (1963), as well as the Isoplot software (Ludwig,

2008), which was also use to plot U-Pb data in Concordia diagrams. Results for AS3 and Plešovice zircon standards are reported in supporting information Table S1 and presented in Figure S1. Altogether, our analyses of AS3 gave a concordant age of 1,102.7 ± 4.6 Ma (2σ) and a weighted average $^{207}Pb/^{206}Pb$ age of 1,101.4 ± 6.6 Ma (2σ; supporting information Figure S1), which are well within uncertainty of the consensus age reported in Paces and Miller (1993). For Plešovice, we obtained a concordant age of 339.3 ± 1.7 Ma (2σ) and a weighted average $^{207}Pb/^{206}Pb$ age of 341.3 ± 9.2 Ma (2σ; supporting information Figure S1), in good agreement with the consensus age reported in Sláma et al. (2008).

Semiquantitative concentrations were also calculated by external normalization to the zircon standard 91500. The range of determined U, Th, and Pb concentrations for AS3 were 159–376, 94–180, and 40–83 ppm (supporting information Table S1), respectively, which agree well with those reported in Paces and Miller (1993). Concerning the range of determined U, Th, and Pb concentrations for Plešovice, they were 268–843, 21–75, and 16–45 ppm (supporting information Table S1), respectively, consistent with concentrations reported in Sláma et al. (2008).

3.2. Handling of U-Pb Data for LA-ICP-MS Traverses

U-Th-Pb data obtained for zircon standards did not exhibit progressive downhole fractionation, which usually results in a continuous drift of elemental ratios, as also noted by Košler and Sylvester (2003). As a consequence, the fractionation is identical for each point of a traverse and this does not require standards and unknowns to be analyzed for the same duration. Moreover, signals acquired during traverses can be cut and considered as separate U-Th-Pb data sets. In order to assess the precision and accuracy of such portions of signal, we have divided a 400 cycle-traverse for each zircon standard (i.e., AS3 and Plešovice) into 8 subsets of 50 cycles. Each subset of AS3 and Plešovice traverses gave $^{206}Pb/^{238}U$ and $^{207}Pb/^{206}Pb$ ages consistent within error with those recommended for these standards (supporting information Table S2). The measured $^{206}Pb/^{238}U$ and $^{207}Pb/^{206}Pb$ ratios determined for each subset of AS3 traverse were associated with uncertainties of 5–7% and 2–4% (supporting information Table S2), respectively, whereas the uncertainty on the same ratios for full traverses were 1–4% and 1–2% (supporting information Table S1), respectively. The measured $^{206}Pb/^{238}U$ and $^{207}Pb/^{206}Pb$ ratios determined for each subset of Plešovice traverse were associated with uncertainties of 2–3% and 4–6% (supporting information Table S2), respectively, whereas the uncertainty on the same ratios for full traverses were 1–4% and 1–3% (supporting information Table S1), respectively. Considered together, the AS3 subsets gave a concordant age of 1,099 ± 14 Ma (2σ), a weighted average $^{206}Pb/^{238}U$ of 1,101 ± 19 Ma (2σ) and a weighted average $^{207}Pb/^{206}Pb$ of 1,098 ± 18 Ma (2σ; supporting information Figure S2), all in good agreement with the consensus age (Paces & Miller, 1993). The subsets for Plešovice traverse gave a concordant age of 338.6 ± 3.0 Ma (2σ), a weighted average $^{206}Pb/^{238}U$ of 338.8 ± 4.1 Ma (2σ) and a weighted average $^{207}Pb/^{206}Pb$ of 329 ± 37 Ma (2σ; supporting information Figure S2), all in good agreement with the consensus age (Sláma et al., 2008). Therefore, cutting the signal acquired during LA-ICP-MS traverses does not affect the accuracy of calculated ages but merely increases the uncertainty associated with them.

The time-resolved signal for each isotope and isotopic ratio measured in Acasta zircons was carefully looked at and the isolation of subsets of data was essentially based on $^{238}U/^{206}Pb$ and/or $^{207}Pb/^{206}Pb$ plateaus and valleys. Internal textures revealed by CL and BSE images, together with variations in Th/U, were parameters that weighted on subset selection in some instances. Once isolated, the U-Th-Pb data for the subsets were plotted in Concordia diagrams, using Isoplot software (Ludwig, 2008), to infer age information. For each and every traverse, the selection of data used to construct Discordia lines was essentially based on the relationship between the zircon texture, the evolution of ages, Th/U, and elemental concentrations throughout the U-Th-Pb isotope analysis. If a datapoint was clearly unrelated to others within a traverse, we either calculated a Concordia age or built a Discordia line to link this datapoint to the origin (i.e., 0 Ma), which is equivalent to considering the measured $^{207}Pb/^{206}Pb$ age. Traverses are better than spot analyses and CL/BSE images in identifying domains of coherent U-Pb systematics but are not immune to issues related to spatial resolution (e.g., coherent zircon domains are smaller than the beam diameter). In such a case, age plateaus and/or valleys may still be identifiable but would correspond to mixed U-Pb isotope information of limited value. To mitigate this issue, we compared obtained ages to those from zircons of the same population and looked at data distribution in Concordia diagrams, in which case it is possible to identify mixing lines. In addition, zircon internal textures were also used as a first-order assessment of genetically unrelated zones sampled during traverses.

4. Results

4.1. Acasta Zircon Internal Textures

As also described in most studies of the AGC (e.g., Bowring & Williams, 1999; Iizuka et al., 2006, 2007; Mojzsis et al., 2014; Reimink et al., 2014), Acasta zircons exhibit various internal textures (Figure 2 and supporting information S3–S5) that can be grouped into five different types. The first type corresponds to zircon crystals that are homogeneously dark in CL images, and bright in BSE images, and with no visible zoning (Figure 2). The second type, which is rare, corresponds to crystals that exhibit few broad zones of different brightness in CL and BSE images that are similar to zircons crystallized under mafic conditions (e.g., Corfu et al., 2003). The third type corresponds to zircons that have homogeneous and dark outer-part (in CL images) that surrounds more or less rounded inner-domains with fine oscillatory zoning (Figure 2), much like magmatic zircons (e.g., Corfu et al., 2003). The thickness of the outer-parts varies greatly from crystal to crystal, and they sometimes appear to be the continuation of their oscillatory-zoned center. The third zircon type corresponds to crystals with best optical quality. The fourth type describes crystals that have consistent zoning from core to rim but, contrary to type 3, this zoning is marked by small domains with patchy and chaotic textures (dark in CL and bright in BSE images), that resemble alteration and/or lattice damaging. The fifth type corresponds to almost entirely mottled crystals that are quite dark in CL images (Figure 2). These crystals also have visible cavities which is generally a sign of advanced metamictization and alteration (e.g., Corfu et al., 2003). Zircon types 3 and 5 greatly dominate in AG09008g (supporting information Figure S3), whereas types 3 and 4 are the most abundant in AG09016 (supporting information Figure S4). With the exception of type 5, which is absent, all types are equally represented in AG09017 (supporting information Figure S5).

Imaged crystals commonly show well-developed cracks that are perpendicular to the zoning and/or have radial distribution (e.g., AG09008g_24, AG09008g_44, AG09017_13, AG09017_40, AG09017_42, AG09016_103, AG09016_131, AG09016_136; supporting information Figures S3–S5). These fractures are visible within bright domains (low U and Th contents) and do not propagate into the darkest zones (high U and Th content) in CL images (Figures 2 and supporting information S3–S5). The formation of these cracks is generally interpreted as resulting from the stress experienced by pristine domains with low U and Th contents, and that is generated by the swelling of surrounding U and Th-rich zones that are at an advanced

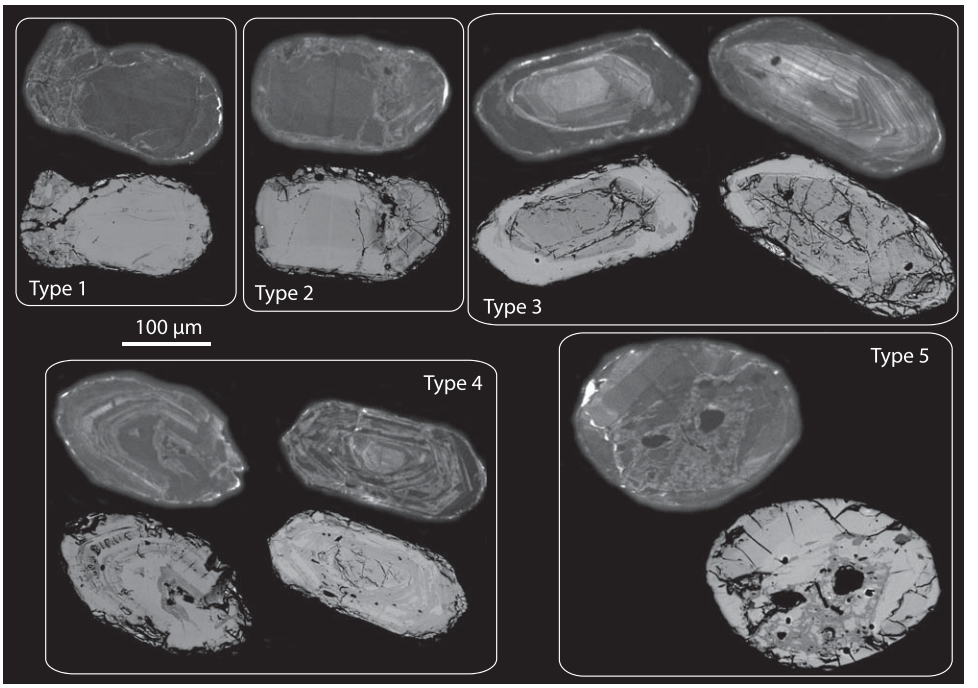

Figure 2. Key textures of Acasta gneiss zircons analyzed herein as revealed by cathodoluminescence (CL) and backscattered electron (BSE) images. For each crystal, the CL image is the upper one and the BSE image is the lower one.

stage of amorphization (Corfu et al., 2003; Hay & Dempster, 2009; Holland & Gottfried, 1955; Lee & Tromp, 1995; Murakami et al., 1991). The optical properties of zircon crystals can, therefore, predict to some degree the pristineness of the U-Th-Pb isotope data that will be acquired, and help further interpret the calculated ages.

4.2. U-Th-Pb Traverses in Acasta Zircons

Results for LA-ICP-MS traverses can be found in supporting information Tables S3–S4 as well as in Figures 3–6 and supporting information Figures S6–S11. The first observation that comes from our analyses is that zones with distinct U-Th-Pb isotope systematics can be identified within single crystals and that this is the case for most of the studied zircons (supporting information Figures S6–S8). When plotted in Concordia diagrams, U-Pb data for isolated zones define internal Discordia lines for most of the analyzed crystals (supporting information Figures S9–S11). Only few zircons display constant U-Th-Pb isotope systematics throughout their entire traverse. Therefore, the presence of internal Discordia lines is a common feature of almost all Acasta zircons. Figure 3 presents the key behaviors that we observed for zircon U-Pb isotope systematics. Some rare crystals exhibited fully concordant U-Pb data (Figure 3a) and/or slight reverse discordance (Figure 3b). Most of the studied zircons had discordant U-Pb data but to several degrees and with various intercepts, which is illustrated in Figures 3c–3e. These latter show little discordance with limited spread (Figure 3c), larger spread going from concordant to quite discordant (Figure 3d), and large spread in discordance with no concordant data (Figure 3e). Some crystals also had two Discordia lines (Figure 3f) that

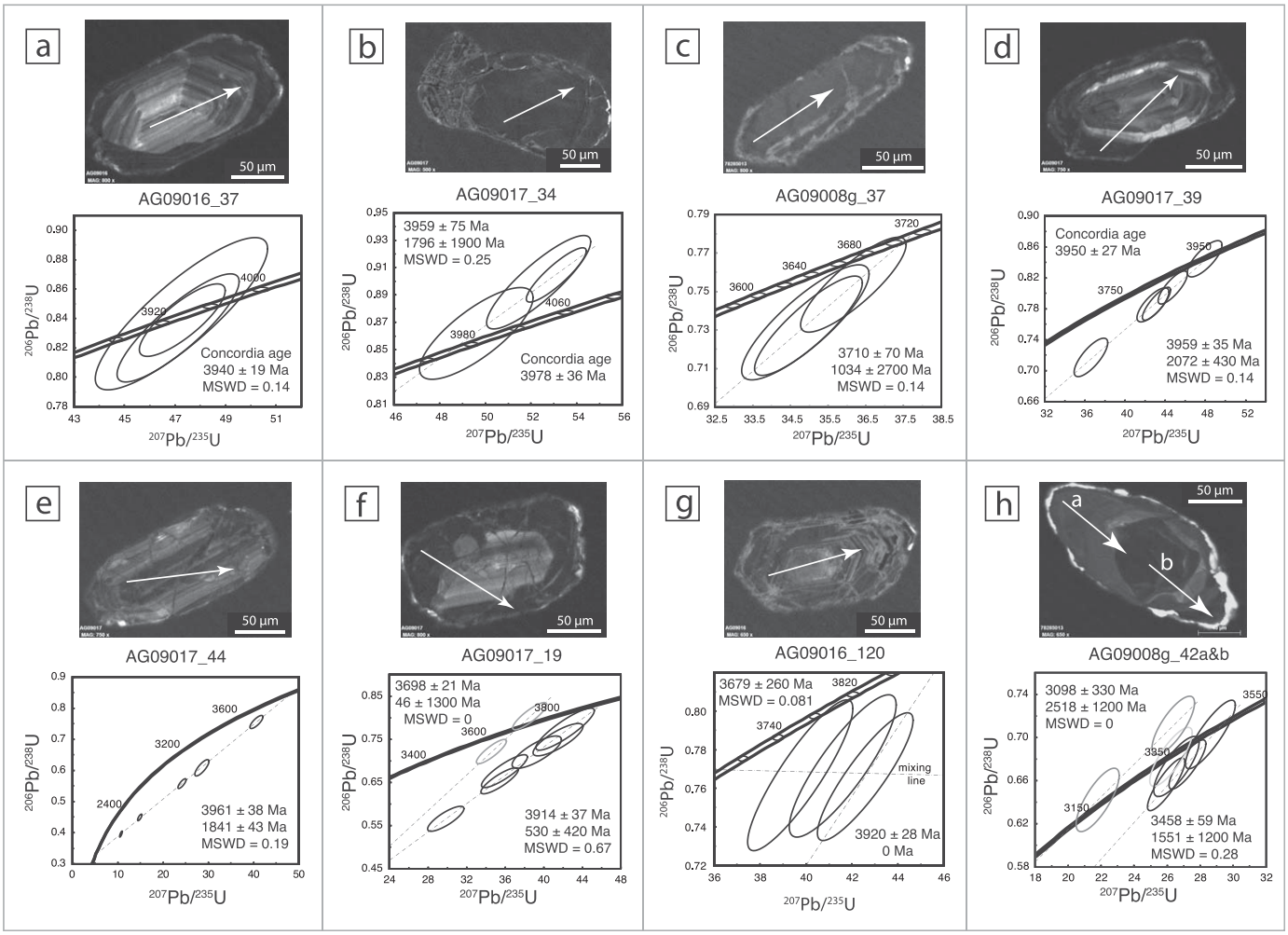

Figure 3. Cathodoluminescence (CL) images and corresponding Concordia diagrams for zircons that display key behaviors observed in analyzed zircon populations. White arrows in CL images represent traverses done by LA-ICP-MS. See text for details.

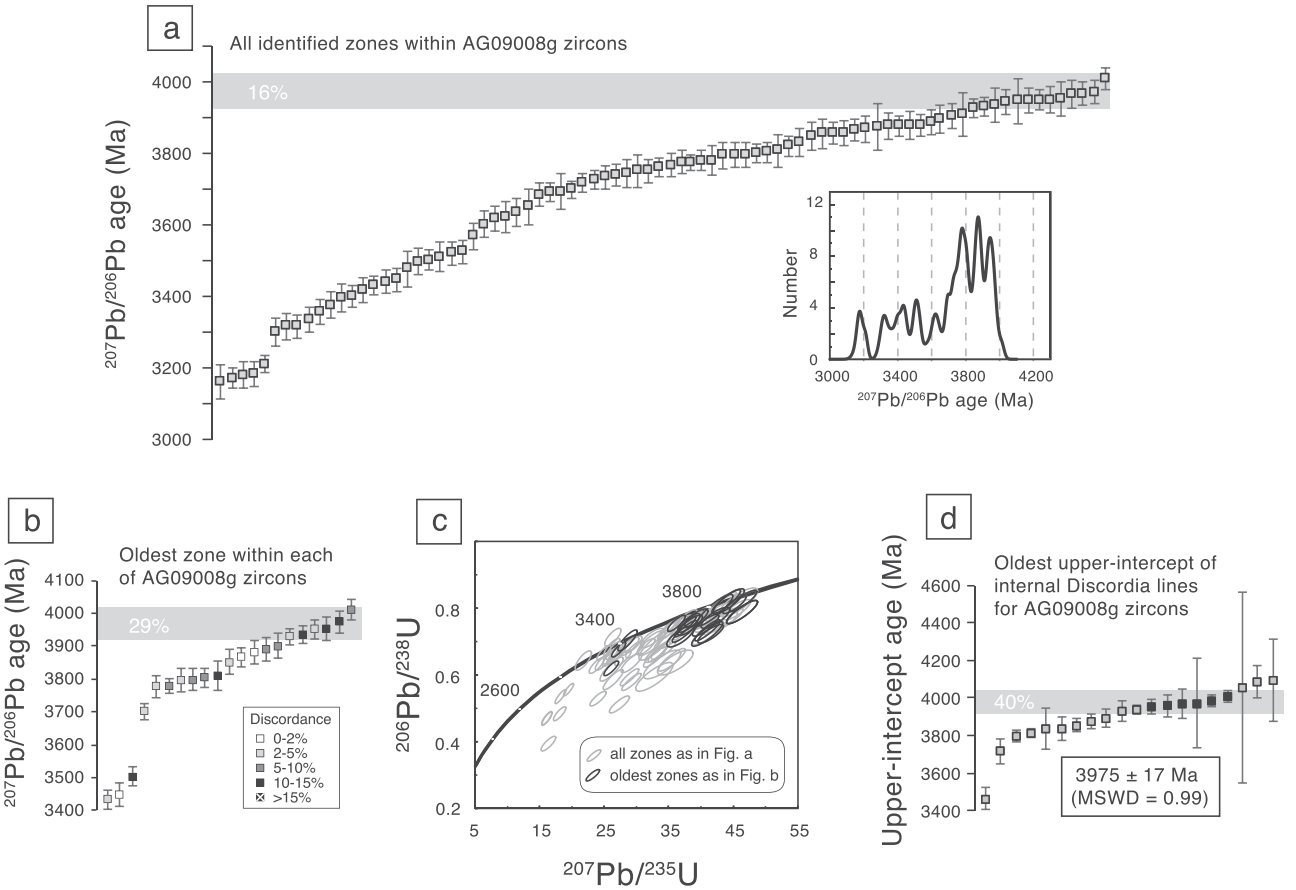

Figure 4. Cumulative plot of (a) ^{207}Pb/^{206}Pb ages, (b) oldest ^{207}Pb/^{206}Pb ages within each zircon crystal, (c) Concordia plot for data presented in Figures 4a and 4b, and (d) oldest Discordia upper-intercept ages for AG09008g zircons. The grey areas in Figures 4a, 4b, and 4d represent the age range for the protolith to the oldest Acasta gneisses (i.e., 3,920–4,020 Ma). Percentages correspond to the amount of datapoints that fall in the grey areas. The inset in Figure 4a is a histogram of ^{207}Pb/^{206}Pb ages presented in the same Figure. The age given in Figure 4d is the weighted average of data corresponding to black squares.

can be attributed to the coexistence of an igneous and a metamorphic domain, and/or patterns corresponding to distinct timings of Pb-loss. The first case is evidenced in AG09017_19 (Figure 3f; supporting information Figure S6B and Tables S3–S4) by the CL texture that shows an oscillatory-zoned center that is sinuously surrounded by a dark outer-part that seems to resorb it. Data for the dark zone (grey spots in Figure 3f) are associated with Th/U $\leq$ 0.1 (supporting information Table S3), whereas data from the central domain (dark spots in Figure 3f) all have Th/U $>$ 0.1 (supporting information Table S3). Note that the upper-intercept age of the Discordia line defined by grey spots in Figure 3f is consistent with that determined in the structureless zircon in Figure 3c, which also has Th/U $<$ 0.1 (supporting information Table S3) that is commonly found in metamorphic zircons (e.g., Hoskin & Schaltegger, 2003; Vavra et al., 1999). Finally, subhorizontal spread has also been observed in some rare instances (Figures 3g and 3h), which could result from mixing between unrelated zircon domains and/or presence of undetected common Pb. We can rule out the latter hypothesis as measured and calculated ^{232}Th/^{238}U ratios commonly agree well with each other, uncertainty-considered, for all identified zones (supporting information Table S3). The following sections present and discuss results sample by sample and in more details.

4.2.1. AG09008g

Zircons from sample AG09008g exhibit ^{207}Pb/^{206}Pb ages that range from 3,160 $\pm$ 48 Ma (2σ; $-$1% discordant) to 4,009 $\pm$ 31 Ma (9%; Figure 4a; supporting information Table S3). Apparent degrees of discordance range from $-$6% to 45% but are mostly moderate as testified to by the average value of 11% for this zircon population. Measured ^{232}Th/^{238}U ratios range from 0.03 to 0.50 and display good agreement with time-integrated ones (i.e., calculated from ^{208}Pb/^{206}Pb) within analytical uncertainty. Uranium concentrations range from 123 to 1,439 ppm, whereas Th concentrations vary between 7 and 586 ppm. Ages, degrees of

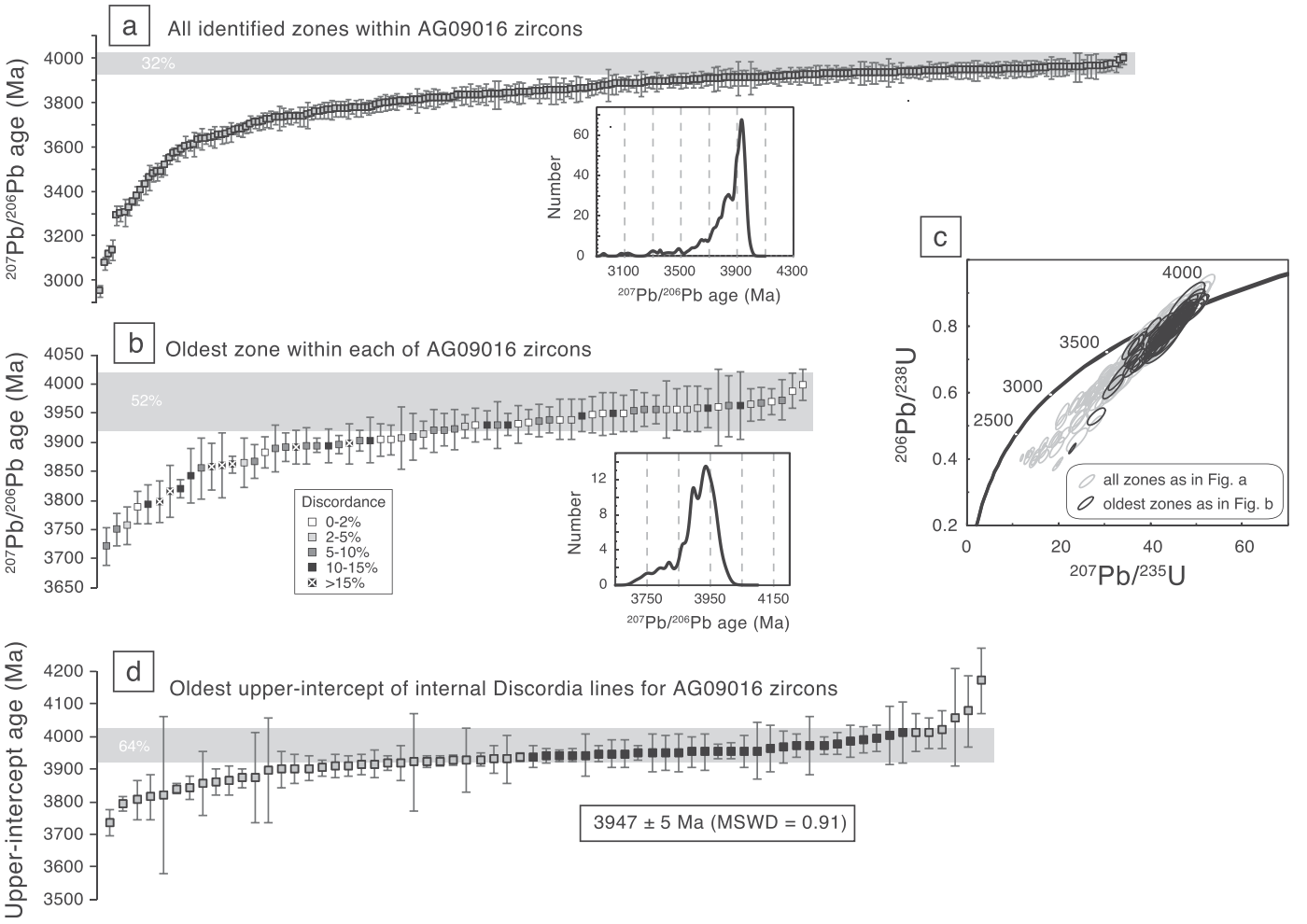

Figure 5. Cumulative plot of (a) ^{207}Pb/^{206}Pb ages, (b) oldest ^{207}Pb/^{206}Pb ages within each zircon crystal, (c) Concordia plot for data presented in Figures 5a and 5b, and (d) oldest Discordia upper-intercept ages for AG09016 zircons (c). The grey areas in Figures 5a, 5b, and 5d represent the age range for the protolith to the oldest Acasta gneisses (i.e., 3,920–4,020 Ma). Percentages correspond to the amount of datapoints that fall in the grey areas. The insets in Figures 5a and 5b are histograms of ^{207}Pb/^{206}Pb ages presented in the same respective Figures. The age given in Figure 5d is the weighted average of data corresponding to black squares.

discordance, Th/U ratios, and elemental concentrations are generally correlated between data from the same crystal such that the youngest is the most discordant, has the lowest Th/U, and the highest U and Th concentrations. However, when data from the entire zircon population are plotted together, these correlations are not visible. Nevertheless, a fan shape that opens up as discordance increases can be seen in a discordance-versus-age diagram.

If we select the oldest zone in each of AG09008g zircons and pool this information together, obtained ^{207}Pb/^{206}Pb ages range from 3,431 ± 28 Ma (4%) to 4,009 ± 31 Ma (9%; Figure 4a; supporting information Table S3). Other parameters vary within more restricted ranges compared to full population. Apparent degrees of discordance vary from 0% to 15% (average = 7%), without correlation with age, nor Th/U ratios. Measured ^{232}Th/^{238}U ratios range from 0.04 to 0.48, and U and Th concentrations range from 183 to 1,036 ppm and from 44 to 366 ppm, respectively.

In a Concordia plot (Figure 4c), it is visible that U-Pb data for AG09008g define a triangular shape indicative of multistage evolution of this zircon population, as observed by other authors (e.g., Bauer et al., 2017; Bowring & Williams, 1999) and consistent with the complex histogram of ages visible in the inset of Figure 4a. Age on or very close to the Concordia spread between 4,000 and 3,100 Ma. U-Pb data that correspond to ages shown in Figure 4b form two groups: (1) a near-concordant to concordant one with ages of 3,800–4,000 Ma, and (2) a near-concordant to concordant one around 3,400 Ma, which is consistent with the drop of ages in Figure 4b.

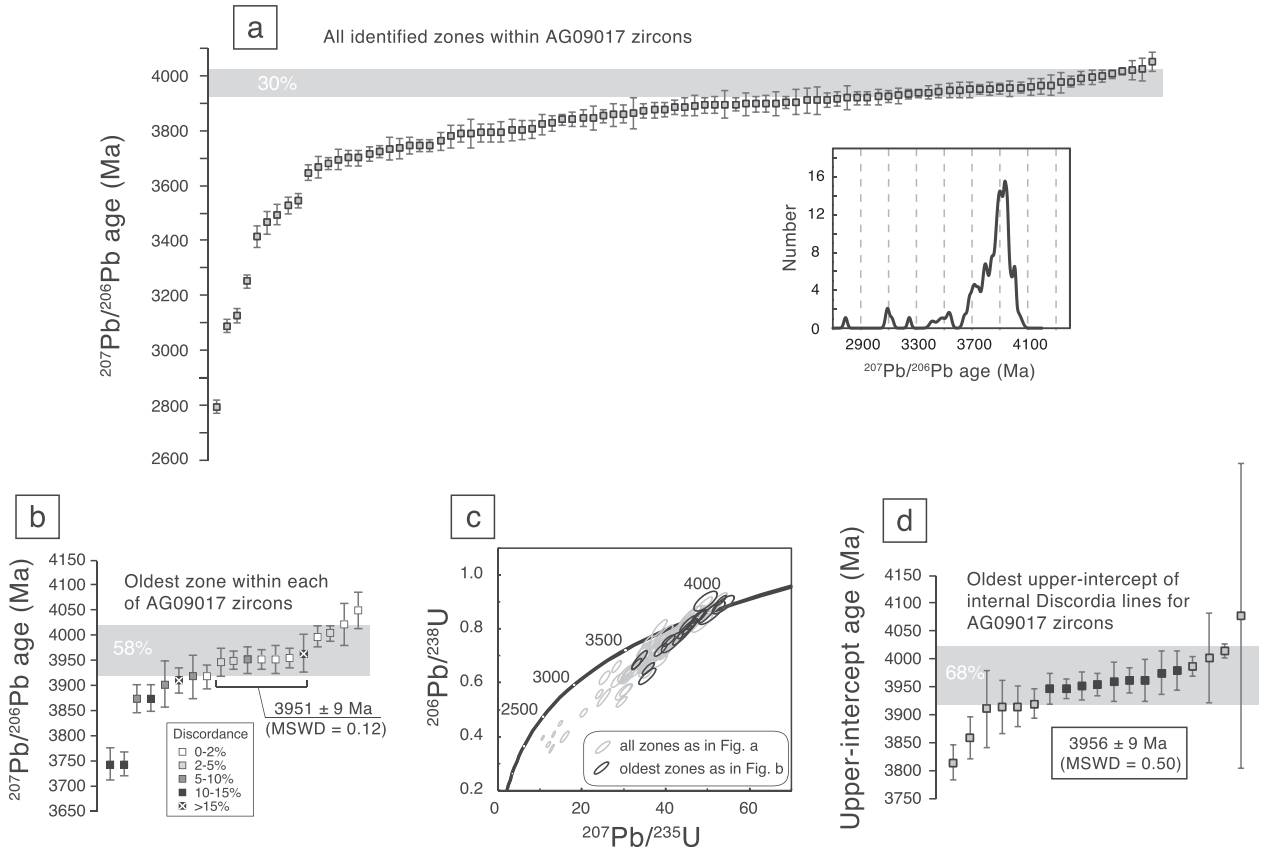

Figure 6. Cumulative plot of (a) ^{207}Pb/^{206}Pb ages, (b) oldest ^{207}Pb/^{206}Pb ages within each zircon crystal, (c) Concordia plot for data presented in Figures 6a and 6b, and (d) oldest Discordia upper-intercept ages for AG09017 zircons (c). The grey areas in Figures 6a, 6b, and 6d represent the age range for the protolith to the oldest Acasta gneisses (i.e., 3,920–4,020 Ma). Percentages correspond to the amount of datapoints that fall in the grey areas. The inset in Figure 6a is a histogram of ^{207}Pb/^{206}Pb ages presented in the same Figure. The age given in Figure 6b is the weighted average of data corresponding to the plateau visible within the grey area whereas the age given in Figure 6d is the weighted average of data corresponding to black squares.

Despite rare exceptions, AG09008g zircons display internal Discordia lines (supporting information Table S4 and Figure S9). Upper-intercept ages range from 4,087 to 3,098 Ma with uncertainties essentially varying between 23 and ~80 Ma, but some extreme, though rare, values up to 510 Ma also exist (supporting information Table S4 and Figure 4d). The large uncertainties in upper-intercept ages are accounted for by the limited spread in ^{206}Pb/^{238}U and ^{207}Pb/^{235}U values among zones of the same crystal, the degrees of discordance of data used to build the Discordia lines, and/or that Discordia lines are sometimes almost parallel to the Concordia curve. Lower-intercept ages range from 3,032 to essentially 0 Ma and are often poorly constrained as illustrated by extreme uncertainties from 210 to 2,800 Ma (supporting information Table S4), which merely derive from the fact that data used to build Discordia lines are not very discordant. The observations on lower-intercept ages indicate that AG09008g zircons underwent U-Pb disturbances at various times from ancient to recent as already observed in previous studies (e.g., Bowring et al., 1989; Guitreau et al., 2012).

4.2.2. AG09016

Zircons from sample AG09016 exhibit ^{207}Pb/^{206}Pb ages that range from 2,949 ± 26 Ma (31%) to 3,997 ± 27 Ma (0%; Figure 5a). Apparent degrees of discordance range from −9% to 53%, but most are moderate as shown by the average value of 12%. Measured ^{232}Th/^{238}U ratios range from 0.02 to 0.97 and are consistent with those calculated from ^{208}Pb/^{206}Pb (time-integrated). Zircons from AG09016 have U concentrations that range from 125 to 3,072 ppm, whereas Th concentrations vary between 15 and 1,794 ppm. Out of the 92 analyses performed on AG09016 zircons, we further selected 67 traverses because those remaining clearly contained a common Pb component. Alike AG09008g zircons, parameters correlate at the scale of single crystals but not when the entire population is considered.

If we select the oldest zone in each of AG09016 zircons and pool this information together, obtained $^{207}Pb/^{206}Pb$ ages range from 3,720 ± 32 Ma (6%) to 3,997 ± 27 Ma (0%; Figure 5b). Much like for AG09008g zircons, other parameters vary within restricted ranges compared to full population. Apparent degrees of discordance range from −5% to 48% (average = 8%). Measured $^{232}Th/^{238}U$ ratios range from 0.04 to 0.62, and U and Th concentrations range from 125 to 977 ppm and from 329 to 609 ppm, respectively. In addition, a broad positive correlation can be seen between $^{207}Pb/^{206}Pb$ ages and $^{232}Th/^{238}U$.

Zircon U-Pb data in Figure 5c define a rough positive correlation with ages on, or very close to, the Concordia curve which spread between 4,000 and 3,700 Ma. This correlation does not regress to zero. The existence of a single broad positive correlation is consistent with the relatively simple histograms visible in the insets of Figures 5a and 5b.

Identified zones within AG09016 zircons define internal Discordia lines for most crystals (supporting information Table S4 and Figure S10). Upper-intercept ages range from 3,460 to 4,172 Ma with precisions commonly ranging from 16 to ~70 Ma, though with rare but larger errors up to 240 Ma (supporting information Table S4 and Figure 5d). Lower-intercept ages range from 2,721 down to ~0 Ma with uncertainties from 63 to 5,900 Ma (supporting information Table S4). Much like AG09008g zircons, those from AG09016 underwent ancient and recent U-Pb disturbances as evidenced by the variable lower-intercept ages.

4.2.3. AG09017

Zircons from sample AG09017 exhibit $^{207}Pb/^{206}Pb$ ages that range from 2,790 ± 25 Ma (27%) to 4,048 ± 36 Ma (–2%; Figure 6a). Apparent degrees of discordance range from −8% to 69%, with a majority being moderate as illustrated by the average value of 11%. Measured $^{232}Th/^{238}U$ ratios range from 0.04 to 0.62 which agrees well with those calculated from $^{208}Pb/^{206}Pb$ (time-integrated) uncertainty considered. Zircons from AG09017 exhibit U concentrations that range from 149 to 3,402 ppm, whereas Th concentrations vary between 32 and 2,219 ppm. Alike AG09008g and AG09016 zircons, ages, degrees of discordance, Th/U ratios, and elemental concentrations correlate at the scale of single crystals but not when the entire population is considered.

If we select the oldest zone in each of AG09017 zircons and pool this information together, obtained $^{207}Pb/^{206}Pb$ ages range from 3,742 ± 32 Ma (13%) to 4,048 ± 36 Ma (–2%; Figure 6b). Much like for AG09008g and AG09016 zircons, Ages, degrees of discordance, Th/U ratios, and elemental concentrations vary within restricted ranges compared to full population. Apparent degrees of discordance range from −8% to 27%, with an average value of 6%, measured $^{232}Th/^{238}U$ ratios range from 0.07 to 0.54 and U and Th concentrations vary from 149 to 1,207 ppm and from 50 to 673 ppm, respectively. In addition, a broad positive correlation can be seen between $^{207}Pb/^{206}Pb$ ages and $^{232}Th/^{238}U$.

U-Pb data for AG09017 zircons define a very broad positive correlation in a Concordia plot (Figure 6c) with ages on, or very close to, the Concordia curve spreading between 4,000 and 3,700 Ma. The correlation does not regress to zero much like for AG09016 data. The distribution of ages displayed in the inset of Figure 6a is consistent with a single broad correlation in Figure 6c.

Identified zones within AG09017 zircons define internal Discordia lines with some displaying good fit (supporting information Table S4 and Figure S11). Upper-intercept ages range from 3,051 to 4,076 Ma with uncertainties commonly ranging from 13 to 90 Ma, except for two Discordia lines that give uncertainties on the upper-intercept ages of 150 and 280 Ma (supporting information Table S4 and Figure 6d). Lower-intercept ages range from 2,926 down to ~0 Ma and associated uncertainties from 43 to 3,200 Ma (supporting information Table S4). Therefore, much like zircons from AG09008g and AG09016, those from AG09017 exhibit evidence for ancient and recent U-Pb disturbances.

5. Discussion

5.1. Retrieval of Zircon Crystallization Ages

Guitreau et al. (2012) showed that zircons from AG09008g, AG09016, and AG09017 exhibit large variations in U-Pb ages despite broadly consistent Lu-Hf isotope systematics. Similar behavior is common in Archean zircons (e.g., Gerdes & Zeh, 2009; Guitreau et al., 2012) and has been reproduced experimentally (Lenting et al., 2010). The U-Pb isotope system is more sensitive to thermal events than the Lu-Hf isotope system merely because Pb is much less retentive than U, Hf, and Lu in zircon (e.g., Cherniak & Watson, 2003) in

addition to being essentially excluded from the lattice during crystallization (e.g., Watson et al., 1997). Consequently, variable U-Pb ages associated with consistent Hf isotope compositions strongly suggest that AG09008g, AG09016, and AG09017 originally had simple zircon populations that formed at 3,982 ± 20, 3,947 ± 13, and 3,974 ± 12 Ma, respectively (Guitreau & Blichert-Toft, 2014; Guitreau et al., 2012). Therefore, one would expect that virtually all zircons can provide information about the timing of original crystallization of the protoliths to the studied Acasta gneisses. However, results for LA-ICP-MS traverses indicate that only 16% of the zones identified in AG09008g zircons have $^{207}Pb/^{206}Pb$ ages that fall within the 3,920–4,020 Ma range (Figure 4a), which corresponds to the lower and the upper-bound for the age of the oldest Acasta gneisses (i.e., Bowring & Williams, 1999; Guitreau et al., 2012, 2014; Iizuka et al., 2007; Mojzsis et al., 2014; Reimink et al., 2014; Stern & Bleeker, 1998). This percentage increases up to 32% for AG09016 zircons and 30% for AG09017 zircons (Figures 5a and 6a). If we, now, consider the oldest coherent zone within each of the analyzed Acasta zircons (i.e., one age per crystal), the percentage of ages that fall within the 3,920–4,020 Ma range rises up to 29%, 52%, and 58% for AG09008g, AG09016, and AG09017, respectively (Figures 4b, 5b, and 6b). The differences in percentages illustrate the fact that studied Acasta zircons have internal age complexities that may challenge the identification of the timing of original crystallization. This is exacerbated by the fact that fine oscillatory-zoned domains, resembling simple magmatic textures, did not always correspond to the oldest domains and did not always have simple and consistent U-Pb systematics, as visible in supporting information Figures S6–S8. In this context, LA-ICP-MS traverses are useful because they can factually identify oldest zones within single crystals and subsequently associate them to crystal textures, in contrast to dating procedures that involve selection of target-zones based on crystal texture revealed by CL/BSE images. It should be noted that the above-given percentages are minimum values as some of the analyzed zircons may be metamorphic and/or have lost information concerning primary crystallization, notably through metamorphic recrystallization. This latter points account for the 3,400 Ma zircons present in AG09008g (Figure 4c). Furthermore, we have purposely chosen a range of target ages for the calculation of percentages, rather than a fixed value, in order to give credit to all groups that studied the Acasta gneisses and because most of the oldest generations of Acasta gneisses contain similarly complex zircon populations (e.g., Bauer et al., 2017; Bowring & Williams, 1999; Iizuka et al., 2007; Mojzsis et al., 2014; Reimink et al., 2016). Therefore, the above-given percentages would certainly change if fixed values were to be targeted but the general increase visible from considering all identified zones to only considering oldest zones would still stand out.

Although powerful at minimizing the issue of U-Pb system reopening, the selection of the oldest zone within a traverse still suffers from the fact that one U-Pb datapoint cannot provide unambiguous crystallization age (e.g., Corfu, 2013; Guitreau & Blichert-Toft, 2014). In this context, the use of internal Discordia lines is relevant because they can provide multiple information. First of all, internal Discordia lines indicate if the studied zircon is made of multiple unrelated components or not, and help interpret multiple age patterns. Second, internal Discordia lines help interpret and/or refine crystallization ages by indicating if discordant data result from recent or ancient U-Pb disturbance(s). If it is recent and that the identified zones are related, the $^{207}Pb/^{206}Pb$ age of the oldest zone confidently depicts the crystallization age of the zircon. If, instead, the disturbance is ancient, the upper-intercept age most likely provides a more accurate crystallization age than the oldest $^{207}Pb/^{206}Pb$ date. When internal Discordia lines are taken into account, 40%, 64%, and 68% of AG09008g, AG09016, and AG09017 zircons, respectively, display upper-intercept ages that fall within the 3,920–4,020 Ma range (Figures 4–6; supporting information Table S4 and Figures S9–S11). If uncertainties associated with upper-intercept ages are considered, these values increase up to 65%, 87%, and 89%, respectively, although some of the reported errors are quite large (Figures 4–6; supporting information Table S4 and Figures S9–S11). Therefore, our results reveal that in a zircon population that developed complexities due to multistage U-Pb disturbances, it is possible to significantly increase the number of crystals that reveal their original crystallization age by using internal Discordia lines built from LA-ICP-MS-traverse data. In spot dating, a large number of U-Pb data are discarded because they are very often discordant and, hence, difficult to interpret, especially in zircon populations like those from Acasta gneisses. The traverse method, hence, significantly reduces the number of analyses needed to establish a sample crystallization age because even discordant data can provide meaningful information, the best example being zircon AG09017_44 (Figure 3e).

The method of dating zircons by LA-ICP-MS traverses, as illustrated in this study, has a great potential for studies of ancient and/or complex crystals because it can alleviate issues related to complex age patterns

and/or U-Pb disturbances. Studies dealing with coupled U-Pb and Lu-Hf isotope systems in detrital zircons are probably the first victim of the one-spot dating approach because these crystals are isolated from their crystallization environment and cannot be treated statistically as is done for igneous crystals (e.g., Guitreau & Blichert-Toft, 2014). Using the traverse approach could improve the accuracy of determined crystallization ages and, in turn, greatly increase the meaningfulness of calculated ε_{Hf} that pertain to source reservoirs. Moreover, in detrital zircon studies, crystals with discordant U-Pb ages are normally discarded, hence, possibly inducing a bias in the final detrital zircon data set. This bias could be greatly reduced by using the method presented in this study. In addition, traverse acquisition times typical varied between 50s and 70s depending on the length of the traverse which does not differ significantly from LA-ICP-MS analyses in spot-mode (e.g., Schoene, 2014). This is much faster than measurements done with other microbeam techniques (i.e., SIMS and SHRIMP) as commonly known (e.g., Košler & Sylvester, 2003; Schoene, 2014). Data from LA-ICP-MS analyses in traverse mode take longer to process than those acquired in spot mode because the former include an additional step to instrumental fractionation correction that is the isolation of plateaus and valleys from the transect signal. This step does not require an extensive amount of time in itself which makes this method a time-worth complement to existing techniques.

A potential problem of the application of the method outlined in this study to detrital zircons is that these crystals are isolated from their crystallization environment and, hence, cannot be compared with each other. Consequently, if a zircon underwent multistage Pb-loss and still exhibit a single Discordia line at the scale of the analytical uncertainty, the ages derived from the upper and lower-intercepts are likely to be spurious. In spot-analyses, discordance filters are often applied so as to remove most discordant data and, hence, eliminate spurious ages. In this context, our approach can be used as an age- mapping technique that objectively reveals the oldest and most concordant age within a crystal, which can then be used as is. However, LA-ICP-MS traverses can go even further in the selection of meaningful ages by allowing the removal of all data in zircons that exhibit Discordia lines with non-zero intercept (i.e., ancient Pb-loss). This filter avoids the possibility of selecting spurious intercepts due to multistage Pb-loss. It is shown in supporting information Figure S12 that this filtering works very well provided that zircon textures are taken into consideration.

5.2. Interpretation of Acasta Zircon U-Pb Ages

It is evident from our results that a large spectrum of ages has been obtained (i.e., $^{207}Pb/^{206}Pb$ ages, upper and lower-intercepts) and that they do not all relate to original igneous crystallization (supporting information Tables S3 and S4 and Figures S9–S11). These ages arguably provide additional information about magmatic and metamorphic events experienced by Acasta gneiss zircons but some of them may also be meaningless. In this section, we assess the meaning of Discordia lines and their associated ages, as well as the $^{207}Pb/^{206}Pb$ age of some of the identified zones, in regard of the known history of the AGC in order to understand the limitations of the approach undertaken in this study.

5.2.1. Ages of Igneous Crystallization

It can be seen in Figures 4–6 that a large number of zircons have ages that fall in the estimated range for original igneous crystallization (3,920–4,020 Ma; Table 1). If upper-intercept ages that cluster as plateaus within the 3,920–4,020 Ma range (black squares in Figures 4–6) are used to estimate original igneous crystallization ages for AG09008g, AG09016, and AG09017, we obtain, respectively, 3,975 ± 17 Ma (N = 6; MSWD = 0.99), 3,947 ± 5 Ma (N = 31; MSWD = 0.91), and 3,956 ± 9 Ma (N = 9; MSWD = 0.50). These ages are consistent with those previously determined in Guitreau et al. (2012) (3,982 ± 20 Ma for AG09008g, 3,947 ± 13 Ma for AG09016, and 3,974 ± 12 Ma for AG09017), which indicates that the method tested in this study provides valid results. When U-Pb data for zones that display the oldest $^{207}Pb/^{206}Pb$ ages are used to estimate crystallization ages for AG09008g, AG09016, and AG09017, we obtain, respectively, 3,959 ± 27 Ma (N = 13; MSWD = 2.0), 3,947 ± 5 Ma (N = 80; MSWD = 0.89), and 3,977 ± 14 Ma (N = 27; MSWD = 5.9; Figure 7). These ages agree well with those previously determined using upper-intercepts. However, there are $^{207}Pb/^{206}Pb$ and upper-intercept ages that are clearly older than the estimated age for crystallization in all Acasta samples studied herein (Figures 4–6; supporting information Tables S3 and S4). This is probably most obvious in AG09017 for which the MSWD is quite large (Figure 7c). Interestingly, when concordant data for AG09016 and AG09017 zircons only are taken into account, they show a spread along Concordia (Figures 7d and 7e) that is larger than what is commonly observed in a simple zircon population. These distributions could be interpreted as reflecting the influence of common Pb, the presence of

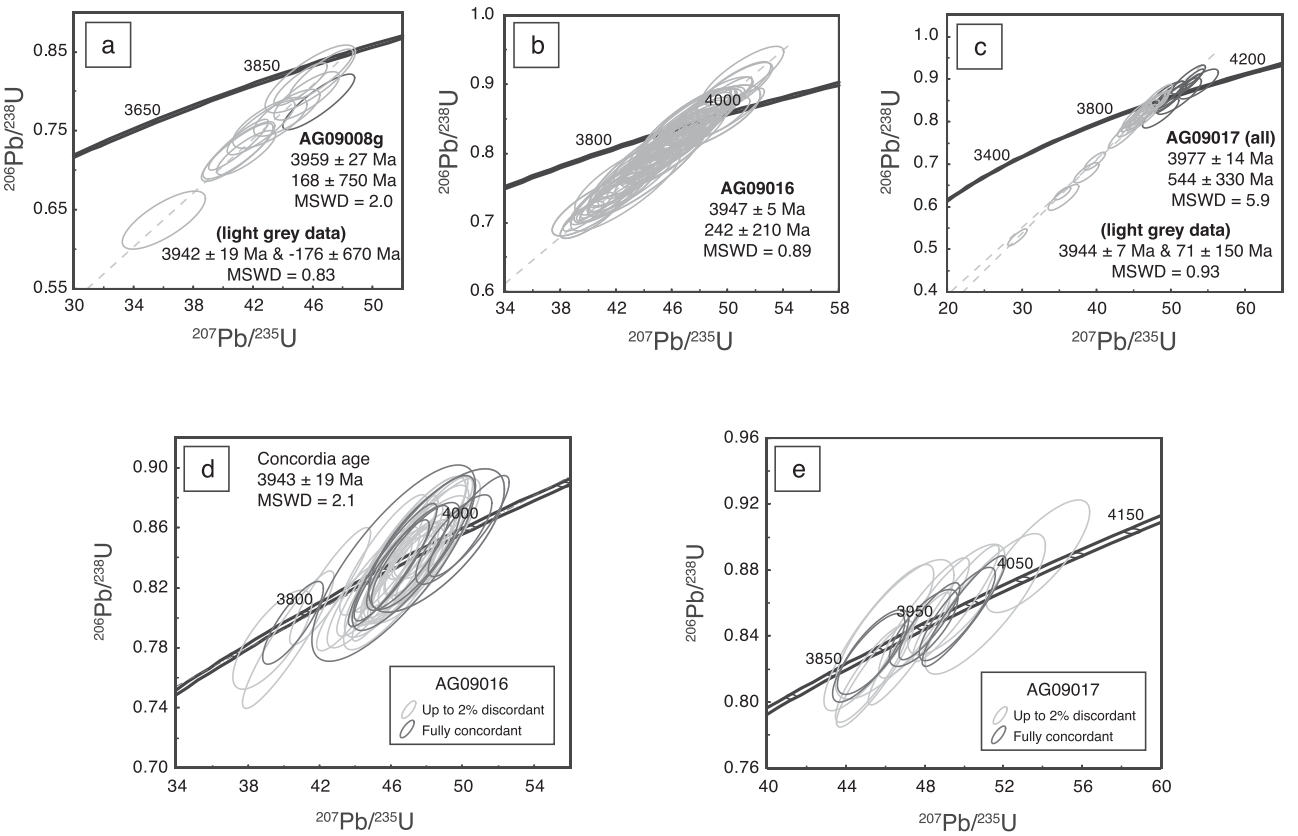

Figure 7. Concordia plot for oldest and most concordant zones (see text for details).

multiple age-components (i.e., magmatic and inherited) and/or artifact of ancient Pb mobility. Contamination by common Pb can be excluded because measured and time-integrated Th/U are consistent in most of the analyzed zircons (supporting information Table S3) and even when discrepancies are observed they are too small to represent a significant change in U-Pb systematics, especially at the scale of analytical uncertainties. The oldest ages may, hence, reflect the actual crystallization age of the Acasta gneisses but could also be artifacts of ancient Pb-addition such as seen in the Napier complex (e.g., Black et al., 1986). Mojzsis et al. (2014) studied Acasta gneisses for their zircon U-Th-Pb isotope systematics coupled with REE and Ti concentrations, as well as textures revealed by CL images, and proposed that zircons with ages >4,000 Ma were inherited and that Acasta gneisses crystallized ~3,920 Myr ago. We note that the oldest $^{207}Pb/^{206}Pb$ ages we obtained for AG09017 correspond to either structureless or very broadly zoned crystals that belong to types 1 and 2 (Figure 2; supporting information Figure S5 and Tables S3 and S4). Therefore, these zircons, or at least part of them, may be inherited from older lithologies. However, AG09017 zircons that contained concordant domains (i.e., AG09017_2, AG09017_27, AG09017_30, AG09017_37, AG09017_39, AG09017_48; supporting information Figure S11) also show evidence for ancient Pb-loss and/or Pb-addition (e.g., AG09017_30), the latter of which results in $^{207}Pb/^{206}Pb$ ratios that corresponds to ages artificially older than those of actual crystallization (e.g., Kusiak et al., 2013a; Williams et al., 1984). Note that zircon AG09017_34, which also belongs to type 1, similarly displays inversely discordant data that correspond to a very old age (Figure 3b and supporting information Figure S5). In contrast, zircons with concordant ages that comply with the estimated time of crystallization display well-preserved fine oscillatory zoning that is typical of type 3 crystals and characteristic of magmatic zircons (Figures 2, supporting information Figure S5 and Tables S3 and S4). Alike AG09017 zircons, those from AG09016 exhibit ancient U-Pb disturbances that resulted in both normal and slight reverse discordance which can account for the spread along Concordia. Yet, the oldest $^{207}Pb/^{206}Pb$ age is found within the core of a zircon that exhibits a structureless texture in CL and BSE images and may, hence, be inherited. This said, concordant data for AG09016 still allow a Concordia age of 3,943 ± 19 Ma (MSWD = 2.1) to be calculated, which agrees with previous estimates. As a consequence, we

surmise that the estimated ages of crystallization deduced from upper-intercept ages are accurate. We cannot exclude either of the hypotheses regarding the distribution of concordant data along Concordia (see Figures 7d and 7e) and, in fact, suggest that this is both due to the presence of inherited cores and an artifact of ancient Pb-mobility. Sample AG09008g also contains older ages than the estimated crystallization age but U-Pb data are commonly more discordant than for AG09016 and AG09017, and zircon textures reveal more radiation damage. These facts altogether with the larger uncertainty associated with AG09008g crystallization age prevent an understanding of the reasons for the age distribution within this sample. However, we assume that it is similar to AG09016 and AG09017.

The upper-intercept age of zircon AG09016_126 is older than the estimated crystallization age of its host-rock, uncertainty-considered (i.e., 4,172 ± 100 Ma). Sample AG09016 is equivalent to sample AC012 from Iizuka et al. (2006) in which a 4.2 Ga core was discovered and, interestingly, the center of zircon AG09016_126 resembles an inherited core. However, zircon magmatic history interpreted from textures revealed by CL/BSE images can be misleading in such ancient and multistage gneisses. Moreover, the corresponding Discordia line is made of three discordant datapoints and, hence, not robust enough to conclude with confidence that zircon AG09016_126 has an inherited Hadean core. This example clearly illustrates the limit of dating zircons by LA-ICP-MS traverses because the Discordia line observed for AG09016_126 may have meaningless intercepts which could arise from undetected presence of common Pb and/or multistage Pb-loss (i.e., ancient and recent). If contamination by common Pb is assessed using the differences observed between measured and time-integrated Th/U ratios (supporting information Table S3), data for zircon AG09016_126 could be seen as having been contaminated by a little amount of common Pb given that all time-integrated ratios are slightly higher than those measured, uncertainty-considered. However, when corrected for common Pb estimated using $^{208}Pb/^{206}Pb$, data for zircon AG09016_126 give upper and lower-intercept ages of 4,156 ± 100 and 2,122 ± 190 Ma (MSWD = 1.5), respectively, which are essentially identical to those obtained with uncorrected data uncertainty considered. Consequently, common Pb cannot account for the Discordia line observed. We cannot conclude on the role of recent Pb-loss because the approach presented here cannot discriminate between specific timings of Pb-loss when U-Pb data form only one Discordia line. The way forward would be to conduct LA-ICP-MS traverses on zircons that were pretreated by chemical abrasion (e.g., Mattinson, 2005), which includes zircon annealing at very high temperature, so as to cure crystal lattice, and subsequent aggressive chemical leaching which removes discordant domains and impurities, such as common Pb. New generations of mass spectrometers such as ICP-MS/MS (e.g., Woods & McCurdy, 2013) may also be useful as they can eliminate ^{204}Hg at mass 204 and would allow common Pb to be more accurately detected, which currently is a major pitfall of zircon U-Pb dating by LA-ICP-MS. The method presented herein, hence, can be improved. Nevertheless, the good agreement between dates obtained in this study and those from the literature indicates that dating zircon using LA-ICP-MS traverses is an interesting complement to already existing techniques and that there is room for improvement.

5.2.2. Recorded Tectono-Metamorphic Events

Zircon can be used to assess metamorphic history of the AGC to a first-order because this mineral has the capability of growing new zones and/or recrystallize under metamorphic conditions. However, this ultimately depends on the pressure-temperature conditions of metamorphism, as well as on the availability of zirconium and the amount of damage accumulated within crystal lattice through U and Th radioactive decay at the time of metamorphism (e.g., Ewing et al., 2003; Holland & Gottfried, 1955). Therefore, zircon can experience a thermal event without recording it. For long-lived zircon crystals, such as those from Acasta gneisses, there should be a large range of sensitivities to disturbances as U and Th concentrations vary between ~100 and ~3,000 ppm and between ~10 and ~2,000 ppm, respectively. As a consequence, what started out as a simple zircon population should have evolved into a complex population that recorded distinct episodes and to various degrees. This is evidenced in Acasta zircons by various crystal textures that correspond to igneous crystallization up to metamorphic recrystallization and alteration (Figure 2; supporting information S3–S5), as well as by variations in Th/U ratios and U-Pb ages (supporting information Tables S3 and S4 and Figures 4–6). The timing of tectono-metamorphic events recorded by Acasta gneiss zircons can be assessed in two ways, which consist in considering (1) Discordia upper-intercept and/or concordant ages for zones or crystals that exhibit metamorphic textures, and (2) Discordia lower-intercept ages (i.e., disturbances to the U-Pb systematics). However, it is obvious from our results (supporting information Table S4 and Figures S9–S11) that the uncertainty on lower-intercepts is commonly quite

large (>200 Ma) which does not allow thermal events to be discussed with the same precision as for crystallization ages. Nevertheless, the precision is still good enough to estimate the disturbance history of some of the studied zircons. It is interesting to note that tectono-metamorphic events deduced from Discordia upper-intercepts and/or concordant ages are always older than those derived from lower-intercepts.

upper-intercept and concordant ages are considered, the zircons we analyzed from AG09008g recorded events corresponding to episodes 5, 6, 7, and 8 (see Table 1), whereas, zircons from AG09016 dominantly recorded the episode 5 (i.e., ~3,750 Ma metamorphism) and very limitedly recorded the episode 6. In contrast, zircons from AG09017 very limitedly recorded episodes 5, 6, and 8. However, all samples exhibit a sort of continuum between about 3,800 up to the actual age of crystallization. We suggest that this distribution is mainly an artifact of ancient U-Pb disturbance and/or multistage Pb-loss (e.g., ancient and recent).

Discordia lines for zircons from all Acasta gneisses studied herein point to the same lower-intercept ages. Considering these latter with uncertainties below 500 Myr, and excluding recent Pb-loss, allow seven tectono-metamorphic events to be identified (supporting information Figure S13 and Table S4). The timing of these events is as follows: (1) 2,800–2,900 Ma, which is equivalent to 9 in Table 1, (2) ~2,400 Ma, (3) 1,700–1,900 Ma, which corresponds to 11 in Table 1, (4) 1,300–1,400 Ma, (5) ~1,100 Ma, (6) 500–700 Ma, and (7) ~200 Ma (supporting information Figure S13). The time constrain on these events is somewhat loose but still good enough to allow resolution of ages from each other. It is interesting to note that some events are visible in more than one sample which is the case for the three oldest events (1, 2, and 3; supporting information Figure S13), the event 3 being the most recorded one among lower-intercepts. The younger ages are somewhat shifted from one sample to the other. It is tempting to try and tie these ages to major geological events that occurred either within the Slave craton or at the scale of Laurentia. However, it should be kept in mind that additional recent Pb-loss in analyzed zircons can modify lower-intercept ages and make them meaningless, which could be the case for some of the identified ages above. Therefore, one should verify the validity of these ages by dating metamorphic minerals (e.g., monazite, apatite) associated with zircons before drawing any conclusion from them. Yet, we note that the first event matches well with an episode of basement formation in the Slave craton (Table 1) (Bauer et al., 2017; Bleeker & Stern, 1997) as well as with the age of the garnets within AG09017 (Maneiro, 2016). The second event matches the breakup of Sclavia (Bleeker, 2003) whereas the third event most likely corresponds to the Wopmay orogen, which was already documented for the AGC, notably by U-Pb ages in apatite (e.g., Sano et al., 1999). The fourth event coincides with limited magmatic activity at the western and eastern margin of Laurentia (e.g., Ernst & Bleeker, 2010) but at the scale of the uncertainties on the lower-intercept ages is not so far off from the massive 1,270 Ma Mackenzie LIP (e.g., Bleeker & Hall, 2007; Ernst & Bleeker, 2010). The Grenville orogen could account for the fifth event, as it occurred in Laurentia and was global (e.g., Karlstrom et al., 2001). The sixth event complies with the rifting of Laurentia that notably induced the formation of some kimberlite fields within the Lake de Gras area (e.g., Bleeker & Hall, 2007).

>LA-ICP-MS traverses in zircons that have advanced radiation-damage textures in CL and BSE images, coupled with Th/U < 0.2, can rarely retrieve original igneous crystallization ages but can provide useful information regarding tectono-metamorphic events, which nevertheless should be further tested independently for validation.

6. Conclusions

In order to obtain more robust U-Pb ages on ancient zircons, we have tested the capability of LA-ICP-MS traverses to identify zones of coherent U-Th-Pb isotope systematics within single crystals from three 3.96 Ga Acasta gneisses previously analyzed by Guitreau et al. (2012). Our results show that using traverses help circumvent issues related to complex zircons (e.g., ancient U-Pb disturbance, presence of multiple age-components). The method presented herein is complementary to existing techniques because it allows better association of age patterns to textures revealed by CL and BSE images and identification of least disturbed domains. It also increases the confidence on the meaning of oldest $^{207}Pb/^{206}Pb$ ages identified within a zircon population through the construction of internal Discordia lines and, in turn, on the interpretation of age distribution in complex zircon populations as evidenced by Acasta gneisses (i.e., crystal inheritance and ancient Pb mobility). The method outlined in this paper further allows retrieval of original crystallization age using internal Discordia upper-intercept age in the case where the studied zircon experienced ancient U-Pb

disturbance. Moreover, crystallization and disturbance histories can be depicted at the scale of single zircon crystals, which is extremely interesting for detrital zircons as they have been isolated from their crystallization environment. Finally, this approach induces higher yield of meaningful data, which means that fewer analyses are needed to establish crystallization ages and, in turn, less dumping of data as commonly done in zircon U-Pb geochronology by LA-ICP-MS.

Acknowledgments
We thank Jean-Marc Hénot for help with CL and BSE image acquisition and Anne-Magali Seydoux-Guillaume for stimulating discussions. We also acknowledge support from the John Templeton Foundation—Ffame Origins program through the Collaborative for Research in Origins (CRiO) program. Martin Guitreau also thanks the Région Auvergne through the Auvergne Fellowship program for financial support. This is Laboratory of Excellence ClerVolc contribution 281. The data used in this study are all available in supporting information Tables S1–S4. We are grateful to Alex Zirakparvar and Jesse Reimink for insightful comments that helped improve the present manuscript, as well as Thorsten Becker for efficient editorial Handling.

References

Allègre, C. J. (1967). Méthode de discussion géochronologique concordia généralisée: Application à la discussion des âges Uranium-Thorium-Plomb discordants. *Earth and Planetary Science Letters*, *2*, 57–66.
Amelin, Y., Lee, D.-C., & Halliday, A. N. (2000). Early-middle Archaean crustal evolution deduced from Lu-Hf and U-Pb isotopic studies of single zircon grains. *Geochimica et Cosmochimica Acta*, *64*(24), 4205–4225.
Amelin, Y., Lee, D. C., Halliday, A. N., & Pidgeon, R. T. (1999). Nature of the Earth's earliest crust from hafnium isotopes in single detrital zircons. *Nature*, *399*(6733), 252–255.
Andersen, T. (2002). Correction of common lead in U-Pb analyses that do not report ^{204}Pb. *Chemical Geology*, *192*(1–2), 59–79.
Bauer, A. M., Fisher, C. M., Vervoort, J. D., & Bowring, S. A. (2017). Coupled zircon Lu-Hf and U-Pb isotopic analyses of the oldest terrestrial crust, the >4.03 Ga Acasta Gneiss Complex. *Earth and Planetary Science Letters*, *458*, 37–48.
Black, L. P., Williams, I. S., & Compston, W. (1986). Four zircon ages from one rock: The history of a 3930 Ma-old granulite from Mount Sones, Enderby Land, Antarctica. *Contributions to Mineralogy and Petrology*, *94*(4), 427–437.
Bleeker, W. (2003). The late Archean record: A puzzle in ca. 35 pieces. *Lithos*, *71*(2–4), 99–134.
Bleeker, W., & Davies, W. J. (1999). The 1991–1996 NATMAP slave province project: Introduction. *Canadian Journal of Earth Sciences*, *36*, 1033–1042.
Bleeker, W., & Hall, B. (2007). The Slave craton: Geological and metallogenic evolution. In W. D. Goodfellow (Ed.), *Mineral deposits of Canada: A synthesis of major deposit-types, district metallogeny, the evolution of geological provinces, and exploration methods* (Spl Publ. 5, pp. 849–879). St. John's, NL: Geological Association of Canada, Mineral Deposits Division.
Bleeker, W., & Stern, R. (1997). The Acasta gneisses: an imperfect sample of Earth's oldest crust. In F. Cook & P. Erdmer (Eds.), *Slave-northern cordillera lithospheric evolution (SNORCLE) transect and cordilleran tectonics workshop meeting* (Lithoprobe Rep. 56, pp. 32–35). Calgary, AB: University of Calgary.
Bowring, S. A., & Housh, T. B. (1995). Earth's early evolution. *Science*, *269*(5230), 1535–1540.
Bowring, S. A., & Williams, I. S. (1999). Priscoan (4.00–4.03 Ga) orthogneisses from northwestern Canada. *Contributions to Mineralogy and Petrology*, *134*(1), 3–16.
Bowring, S. A., Williams, I. S., & Compston, W. (1989). 3.96 Ga gneisses from the Slave province, Northwest-Territories, Canada. *Geology*, *17*(11), 971–975.
Catanzaro, E. J., & Kulp, J. L. (1964). Discordant zircons from the Little Belt (Montana), Beartooth (Montana) and Santa Catalina (Arizona) Mountains. *Geochimica et Cosmochimica Acta*, *28*(1), 87–124.
Cherniak, D. J., & Watson, E. B. (2003). Diffusion in zircon. *Reviews in Mineralogy and Geochemistry*, *53*(1), 113–143.
Ernst, R., & Bleeker, W. (2010). Large igneous provinces (LIPs), giant dyke swarms, and mantle plumes: Significance for breakup events within Canada and adjacent regions from 2.5 Ga to the Present. *Canadian Journal of Earth Sciences*, *47*(5), 695–739.
Connelly, J. N. (2001). Degree of preservation of igneous zonation in zircon as a signpost for concordancy in U-Pb geochronology. *Chemical Geology*, *172*(1–2), 25–39.
Corfu, F. (2013). A century of U-Pb geochronology: The long quest towards concordance. *Geological Society of America Bulletin*, *125*(1–2), 33–47. https://doi.org/10.1130/B30698.1
Corfu, F., Hanchar, J. M., Hoskin, P. W. O., & Kinny, P. (2003). Atlas of zircon textures. *Reviews in Mineralogy and Geochemistry*, *53*(1), 469–500.
Ewing, R. C., Meldrum, A., Wang, L., Weber, W. J., & Corrales, L. R. (2003). Radiation effects in zircon. *Reviews in Mineralogy and Geochemistry*, *53*(1), 427–467.
Gehrels, G. (2014). Detrital zircon U-Pb geochronology applied to tectonics. *Annual Review of Earth and Planetary Sciences*, *42*(1), 127–149.
Gerdes, A., & Zeh, A. (2009). Zircon formation versus zircon alteration: New insights from combined U-Pb and Lu-Hf in-situ LA-ICP-MS analyses, and consequences for the interpretation of Archean zircon from the central zone of the Limpopo belt. *Chemical Geology*, *261*(3–4), 230–243.
Guitreau, M., & Blichert-Toft, J. (2014). Implications of discordant U-Pb ages on Hf isotope studies of detrital zircons. *Chemical Geology*, *385*, 17–25.
Guitreau, M., Blichert-Toft, J., Martin, H., Mojzsis, S. J., & Albarède, F. (2012). Hafnium isotope evidence from Archean granitic rocks for deep mantle origin of continental crust. *Earth and Planetary Science Letters*, *337–338*, 211–223.
Guitreau, M., Blichert-Toft, J., Mojzsis, S. J., Roth, A. S. G., Bourdon, B., Cates, N. L., et al. (2014). Lu-Hf isotope systematics of the Hadean-Eoarchean Acasta Gneiss complex (Northwest territories, Canada). *Geochimica et Cosmochimica Acta*, *135*, 251–269.
Harrison, M. T. (2009). The Hadean crust: Evidence from >4 Ga zircons. *Annual Review of Earth and Planetary Sciences*, *37*(1), 479–505.
Hay, D. C., & Dempster, T. J. (2009). Zircon behavior during low-temperature metamorphism. *Journal of Petrology*, *50*(4), 571–589.
Hiess, J., Condon, D. J., McLean, N., & Noble, S. R. (2012). ^{238}U/^{235}U systematics in terrestrial uranium-bearing minerals. *Science*, *335*(6076), 1610–1614.
Hodges, K. V., Bowring, S. A., Coleman, D. S., Hawkins, D. P., & Davide, K. L. (1995). Multi-stage thermal history of the ca. 4.0 Ga Acasta gneisses. *Eos transactions AGU*, 76(17), Abstract F708.
Holland, H. D., & Gottfried, D. (1955). The effect of nuclear radiation on the structure of zircon. *Acta Crystallographica*, *8*(6), 291–300.
Hoskin, P. W. O., & Schaltegger, U. (2003). The composition of zircon and igneous and metamorphic petrogenesis. *Reviews in Mineralogy and Geochemistry*, *53*(1), 27–62.
Iizuka, T., Horie, K., Komiya, T., Maruyama, S., Hirata, T., Hidaka, H., et al. (2006). 4.2 Ga zircon xenocryst in an Acasta gneiss from northwestern Canada: Evidence for early continental crust. *Geology*, *34*(4), 245–248.
Iizuka, T., Komiya, T., Johnson, S. P., Kon, Y., Maruyama, S., & Hirata, T. (2009). Reworking of Hadean crust in the Acasta gneisses, northwestern Canada: Evidence from in-situ Lu-Hf isotope analysis of zircon. *Chemical Geology*, *259*(3–4), 230–239.
Iizuka, T., Komiya, T., Ueno, Y., Katayama, I., Uehara, Y., Maruyama, S., et al. (2007). Geology and zircon geochronology of the Acasta Gneiss Complex, northwestern Canada: New constraints on its tectonothermal history. *Precambrian Research*, *153*(3–4), 179–208.

Ireland, T. R., & Williams, I. S. (2003). Considerations in zircon geochronology by SIMS. *Reviews in Mineralogy and Geochemistry*, *53*(1), 215–241.

Jaffey, A. H., Flynn, K. F., Glendenin, L. E., Bentley, W. C., & Essling, A. M. (1971). Precision measurement of half-lives and specific activities of 235U and 238U. *Physical Review C*, *4*, 1889–1906.

Karlstrom, K. E., Åhäll, K.-I., Harlan, S. S., Williams, M. L., McLelland, J., & Geissman, J. W. (2001). Long-lived (1.8–1.0 Ga) convergent orogen in southern Laurentia, its extensions to Australia and Baltica, and implications for refining Rodinia. *Precambrian Research*, *111*(1–4), 5–30.

King, J. E. (1986). The metamorphic internal zone of Wopmay orogen (early proterozoic), Canada: 30 km of structural relief in a composite section based on plunge projection. *Tectonics*, *5*(7), 973–994. https://doi.org/10.1029/TC005i007p00973

Koshida, K., Ishikawa, A., Iwamori, H., & Komiya, T. (2016). Petrology and geochemistry of mafic rocks in the Acasta Gneiss complex: Implications for the oldest mafic rocks and their origin. *Precambrian Research*, *283*, 190–207.

Košler, J., & Sylvester, P. J. (2003). Present trends and the future of zircon in Geochronology: Laser ablation ICPMS. *Reviews in Mineralogy and Geochemistry*, *53*(1), 243–275.

Kovaleva, E., & Klötzli, U. (2017). NanoSIMS study of seismically deformed zircon: Evidence of Y, Yb, Ce, and P redistribution and resetting of radiogenic Pb. *American Mineralogist*, *102*(6), 1311–1327.

Kusiak, M. A., Whitehouse, M. J., Wilde, S. A., Dunkley, D. J., Menneken, M., Nemchin, A. A., et al. (2013a). Changes in zircon chemistry during Archean UHT metamorphism in the Napier Complex, Antarctica. *American Journal of Science*, *313*, 933–967.

Kusiak, M. A., Whitehouse, M. J., Wilde, S. A., Nemchin, A. A., & Clark, C. (2013b). Mobilization of radiogenic Pb in zircon revealed by ion imaging: Implications for early Earth geochronology. *Geology*, *41*, 291–294.

Lee, J. K. L., & Tromp, J. (1995). Self-induced fracture generation in zircon. *Journal of Geophysical Research*, *100*(B9), 17753–17770. https://doi.org/10.1029/95JB01682

Lenting, C., Geisler, T., Gerdes, A., Kooijman, E., Scherer, E. E., & Zeh, A. (2010). The behavior of the Hf isotope system in radiation-damaged zircon during experimental hydrothermal alteration. *American Mineralogist*, *95*(8–9), 1343–1348.

LeRoux, L. J., & Glendenin, L. E. (1963). Half-life of ^{232}Th. In F. L. Warren (Ed.), *National conference on nuclear energy, Application of isotopes and radiation. Proceedings of the national conference on nuclear energy* (pp. 83–94). Pelindaba, South Africa: South African Atomic Energy Board.

Ludwig, K. R. (2008). *User's manual for Isoplot 3.6: A geochronological toolkit for Microsoft Excel* (Spec. Pub. 4). Berkeley, CA: Berkeley Geochronology Center.

Maneiro, K. A. (2016). *Development of a detrital garnet geochronometer and the search for Earth's oldest garnet* (PhD thesis, 354 pp.). Boston, MA: Boston University Libraries.

Mattinson, J. M. (2005). Zircon U-Pb chemical abrasion ("CA-TIMS") method: Combined annealing and multi-step partial dissolution analysis for improved precision and accuracy of zircon ages. *Chemical Geology*, *220*(1–2), 47–66.

Mojzsis, S. J., Cates, N. L., Caro, G., Trail, D., Abramov, O., Guitreau, M., et al. (2014). Component geochronology in the polyphase ca. 3920 Ma Acasta gneiss. *Geochimica et Cosmochimica Acta*, *133*, 68–96.

Möller, A., O'Brien, P. J., Kennedy, A., & Kröner, A. (2003). Linking growth episodes of zircon and metamorphic textures to zircon chemistry: An example from the ultrahigh-temperature granulites of Rogaland (SW Norway). *Geological Society, Special Publications*, *220*(1), 65–81.

Moorbath, S., Whitehouse, M. J., & Kamber, B. S. (1997). Extreme Nd-isotope heterogeneity in the early Archaean–fact or fiction? Case histories from northern Canada and West Greenland. *Chemical Geology*, *135*(3–4), 213–231.

Murakami, T., Chakoumakos, B. C., Ewing, R., Lumpkin, G. R., & Weber, W. J. (1991). Alpha-decay event damage in zircon. *American Mineralogist*, *76*, 1510–1532.

Paces, J. B., & Miller, J. D. Jr. (1993). Precise U-Pb ages of Duluth complex and related mafic intrusions, Northeastern Minnesota: Geochronological insights to physical, petrogenetic, paleomagnetic, and tectonomagmatic processes associated with the 1.1 Ga midcontinent rift system. *Journal of Geophysical Research*, *98*(B8), 13997–14013. https://doi.org/10.1029/93JB01159

Paquette, J. L., Piro, J. L., Devidal, J. L., Bosse, V., Didier, A., Sannac, S., et al. (2014). Sensitivity enhancement in LA-ICP-MS by N2 addition to carrier gas: Application to radiometric dating of U-Th-bearing minerals. *Agilent ICP-MS Journal*, *58*, 4–5.

Pidgeon, R. T., Nemchin, A. A., & Whitehouse, M. J. (2017). The effect of weathering on U-Th-Pb and oxygen isotope system of ancient zircons from the Jack Hills, Western Australia. *Geochimica et Cosmochimica Acta*, *197*, 142–166.

Reimink, J. R., Chacko, T., Stern, R. A., & Heaman, L. M. (2014). Earth's earliest evolved crust generated in an Iceland-like setting. *Nature Geoscience*, *7*(7), 529–533.

Reimink, J. R., Chacko, T., Stern, R. A., & Heaman, L. M. (2016). The birth of a cratonic nucleus: Lithogeochemical evolution of the 4.02–2.94 Ga Acasta Gneiss complex. *Precambrian Research*, *281*, 453–472.

Roth, A. S. G., Bourdon, B., Mojzsis, S. J., Rudge, J. F., Guitreau, M., & Blichert-Toft, J. (2014). Combined 147,146Sm–143,142Nd constraints on the longevity and residence time of early terrestrial crust. *Geochemistry, Geophysics, Geosystems*, *15*, 2329–2345. https://doi.org/10.1002/2014GC005313

Sano, Y., Terada, K., Hidaka, H., Yokoyama, K., & Nutman, A. P. (1999). Palaeoproterozoic thermal events recorded in the 4.0 Ga Acasta gneiss, Canada: Evidence from SHRIMP U-Pb dating of apatite and zircon. *Geochimica et Cosmochimica Acta*, *63*(6), 899–905.

Schmitz, M. D., Bowring, S. A., & Ireland, T. R. (2003). Evaluation of Duluth complex anorthositic series (AS3) zircon as a U-Pb geochronological standard: New high-precision isotope dilution thermal ionization mass spectrometry results. *Geochimica et Cosmochimica Acta*, *67*(19), 3665–3672.

Schoene, B. (2014). U-Th-Pb geochronology. In H. Holland & K. Turekian (Eds.), *Treatise on geochemistry* (2nd ed., Chap. 4.10, pp. 341–378). Oxford, UK: Elsevier.

Sláma, J., Košler, J., Condon, D. J., Crowley, J. L., Gerdes, A., Hanchar, J. M., et al. (2008). Plesovice zircon: A new natural reference material for U-Pb and Hf isotopic microanalysis. *Chemical Geology*, *249*(1–2), 1–35.

Stern, R. A., & Bleeker, W. (1998). Age of the world's oldest rocks refined using Canada's SHRIMP: The Acasta gneiss complex, Northwest Territories, Canada. *Geoscience Canada*, *25*, 27–31.

Timms, N. E., Kinny, P. D., & Reddy, S. M. (2006). Enhanced diffusion of uranium and thorium linked to crystal plasticity in zircon. *Geochemical Transactions*, *7*(10), 1–16.

Valley, J. W., Reinhard, D. A., Cavosie, A. J., Ushikubo, T., Lawrence, D. F., Larson, D. J., et al. (2015). Nano- and micro-geochronology in Hadean and Archean zircons by atom-probe tomography and SIMS: New tools for old minerals. *American Mineralogist*, *100*(7), 1355–1377.

Vavra, G., Schmid, R., & Gebauer, D. (1999). Internal morphology, habit and U-Th-Pb microanalysis of amphibolite-to-granulite- facies zircons: Geochronology of the Ivrea zone (Southern Alps). *Contributions to Mineralogy and Petrology*, *134*(4), 380–404.

Watson, E. B., Chemiak, D. J., Hanchar, J. M., Harrison, T. M., & Wark, D. A. (1997). The incorporation of Pb into zircon. *Chemical Geology*, *141*(1–2), 19–31.

Wetherill, G. W. (1956). Discordant uranium-lead ages, I. *EOS, Transactions American Geophysical Union*, *37*(3), 320–326.

Wetherill, G. W. (1963). Discordant uranium-lead ages: 2. Discordant ages resulting from diffusion of lead and uranium. *Journal of Geophysical Research*, *68*(10), 2957–2965. https://doi.org/10.1029/JZ068i010p02957

Wiedenbeck, M., Allé, P., Corfu, F., Griffin, W. L., Meier, M., Oberli, F., et al. (1995). Three natural zircon standards for U–Th–Pb, Lu–Hf, trace element and REE analyses. *Geostandards Newsletters*, *19*(1), 1–23.

Willbold, M., Mojzsis, S. J., Chen, H.-W., & Elliott, T. (2015). Tungsten isotope composition of the Acasta Gneiss complex. *Earth and Planetary Science Letters*, *419*, 168–177.

Williams, I. S., Compston, W., Black, L. P., Ireland, T. R., & Foster, J. J. (1984). Unsupported radiogenic Pb in zircon: A cause of anomalously high Pb-Pb, U-Pb and Th-Pb ages. *Contributions to Mineralogy and Petrology*, *88*(4), 322–327.

Woods, G. D., & McCurdy, E. (2013). Triple-quadrupole ICP-MS provides improved performance for difficult polyatomic and isobaric overlaps on lead isotopes. *Spectroscopy*, *28*(11), 28–34.

Zirakparvar, N. A. (2015). Cathodoluminescence guided zircon Hf isotope depth profiling: Mobilization of the Lu-Hf system during (U)HP rock exhumation in the Woodlark Rift, Papua New Guinea. *Lithos*, *220–223*, 81–96.

Zirakparvar, N. A., Setera, J., Mathez, E., Vantongeren, J., & Fossum, R. (2017). The pre-Atlantic Hf isotope evolution of the east Laurantian continental margin: Insights from zircon in basement rocks and glacial tillites from northern New Jersey and southeastern New York. *Lithos*, *272–273*, 69–83.